https://doi.org/10.5194/egusphere-2026-112
Preprint. Discussion started: 16 January 2026

Persistent EarthCARE underflight studies of the ITCZ and organized convection (PERCUSION): Contribution to EarthCARE Validation

Silke Groß[1], Florian Ewald[1], Bjorn Stevens[2], Martin Wirth[1], Georgios Dekoutsidis[1], André Ehrlich[3], Dimitra Kouklaki[4], Konstantin Krüger[1], Sophie Rosenburg[3], Lea Volkmer[5], Jonas v. Bismark[6], Lutz Hirsch[2], Anna E. Luebke[3], Eleni Marinou[4], Bernhard Mayer[5], Montserrat Pinol Sole[6], Manfred Wendisch[3], Julia Windmiller[2], Vassilis Amiridis[4], Rob Koopman[6], Takuji Kubota[7], Markus Rapp[1]

[1]Institue of Atmospheric Physics, German Aerospace Center (DLR), Oberpfaffenhofen, Germany
[2]Max Planck Institute for Meteorology, Hamburg, Germany
[3] Leipzig Institute for Meteorology, Leipzig University, Leipzig, Germany
[4] National Observatory of Athens, Athens, Greece
[5]Ludwig-Maximilians-Universität München, Munich, Germany
[6]European Space Agency (ESA), Noordwijk, Netherlands
[7]Earth Observation Research Center, Japan Aerospace Exploration Agency (JAXA), Tsukuba-city, Japan

Correspondence to: Silke Groß (silke.gross@dlr.de)

Abstract.

In May 2024, the **Earth C**louds, **A**erosols and **R**adiation **E**xplorer (EarthCARE) satellite was launched. For the first time a satellite combines two active instruments, i.e., the Atmospheric Lidar and the Cloud Profiling Radar, together with two passive instruments, a multi-spectral imager and a broad-band radiometer, on one single spacecraft platform. EarthCARE is thus the most complex satellite mission to date to for collocated aerosol, cloud, radiation and precipitation measurements. To utilize the data collected by the EarthCARE mission to its full extent and to support and quantify the data quality and measurement uncertainty, careful and holistic validation activities are needed. For this purpose, we set up an airborne instrument payload on the German High Altitude and LOng-range research aircraft (HALO), which is similar to the EarthCARE instrumentation. We used this payload during an extensive measurement campaign in summer and fall 2024 in the tropic, sup-tropic and mid- to high-latitudes targeting to validate the EarthCARE measurements and data products early in its commissioning phase. With 33 passes under the EarthCARE satellite during 30 research flights we were able to address target scenes that have been identified by the EarthCARE algorithm developers to be of importance for the validation of the mission, and to assure the retrieval performance under different meteorological conditions and aerosol-cloud situations.

https://doi.org/10.5194/egusphere-2026-112
Preprint. Discussion started: 16 January 2026

1. Introduction

Despite major progress in understanding atmospheric aerosol and cloud processes to decrease uncertainties and enhance confidence in how they interact with the Earth's climate system, aerosol particles and clouds, their interaction and feedback mechanisms on the radiative energy budget and on precipitation formation significantly contribute to the largest uncertainties in climate change projections (IPCC, 2023). A significant contribution to improve our understanding of aerosol and cloud processes has been made by two satellite missions that focused on aerosol and cloud vertical profiling by lidar and radar, respectively; NASA's Cloud Aerosol Lidar Pathfinder Satellite Observation (CALIPSO) mission (Winker et al., 2010) and NASA's Cloudsat mission (Stephens et al., 2008). Launched jointly in 2006, they provided detailed information on the global vertical structure of aerosol particles and clouds. Especially their synergistic use provided new insights to aerosol and cloud research and to aerosol-cloud interactions (Stephens et al., 2018). The significant benefit of the satellite missions could only be ensured by securing the quality and accuracy of their data through extensive and repeatedly validation efforts throughout the lifetime of the mission.

Following the Committee on Earth Observation Satellites (CEOS) nomenclature, validation is defined as the process of assessing the quality of data products by independent means (ISO/TS 19159- 1:2014). This can include the assessment of the quality of the data products, the quality of the measurements itself, and the representativeness of the data. The independent means are defined as data from instruments external to the mission but measuring the same geophysical quantity as the satellite sensor that is to be validated. A review and summary of the general approaches, challenges and limitations for the validation of satellite missions (Langsdale et al., 2025) and with a focus on profiling missions (Amiridis et al., 2025) highlight the importance of reliable and comparable independent data.

Airborne measurements with the same or similar payload as the satellite instruments have been shown to be a valuable tool for satellite validation especially of profiling instruments, i.e. lidar and radar. For the validation of Cloud-Aerosol LIdar with Orthogonal Polarization (CALIOP) onboard of CALIPSO, a total of 147 underflights with an airborne high spectral resolution lidar (HSRL) were performed during the lifetime of the mission, which proofed to have the most impact in measurement validation and algorithm improvement. These measurements were used to assess the quality of the CALIOP Level 1 products early in the mission's lifetime (Rogers et al., 2011), and served for quality assessments of algorithm improvements throughout CALIOP's lifetime (Getzewich et al., 2018; Kar et al., 2018). Airborne HSRL measurements were used to assess CALIOP Level 2 products, e.g., the aerosol particle backscatter and extinction coefficient, the optical depth, aerosol type classification, and the layer detection sensitivity (Burton et al., 2013; Kacenelenbogen et al., 2014; Rogers et al., 2014). To validate both instrument systems, the CALIPSO and Cloudsat Validation Experiment (CC-VEX) took place immediately after the commissioning phase of both satellites (McGill, et al., 2007), deploying an elastic backscatter lidar and a W-band cloud radar on the ER-2 aircraft. During the Canadian Cloudsat-CALIPSO Validation Project airborne Ku-band radar measurements were performed for validation purposes (Barker et al., 2008). ESA's Earth Explorer wind lidar mission AEOLUS highly benefited from airborne validation campaigns. Doppler wind lidars were deployed to prepare for the mission (Lemmerz et al., 2023) and

https://doi.org/10.5194/egusphere-2026-112
Preprint. Discussion started: 16 January 2026

to validate the AEOLUS wind and aerosol product with independent technique (Bedka et al., 2021; Witschas et al., 2020; Witschas et al., 2022). A large impact in the preparation (Lux et al., 2018) and the improvement of retrievals (Lux et al., 2022) was made by the development and deployment of an airborne demonstrator of the spaceborne system (Reitebuch et al., 2009; Paffrath et al., 2009). Beyond the validation of active sensors, airborne demonstrators have been found to be also a valuable tool for passive satellite missions (King et al., 1996).

Motivated by the benefit of airborne demonstrators (Fix et al., 2016), we set up an EarthCARE-like payload consisting of similar instruments like the one on EarthCARE (Stevens et al., 2019) on the German High Altitude and LOng-range research aircraft (HALO) (Krautstrunk and Giez, 2012) to prepare for the EarthCARE (**Earth C**louds, **A**erosols and **R**adiation **E**xplorer) mission and for post launch validation measurements. We used the measured data for the development of independent algorithms, e.g., its lidar-based aerosol type classification (Groß et al., 2013; Groß et al., 2015), aerosol type separation (Gutleben et al., 2022), lidar-radar target classification (Marinou et al., 2020). Furthermore, we developed and tested synergistic radar-lidar retrievals to derive ice and mixed-phase cloud microphysical properties (Cazenave et al., 2019; Aubry et al., 2024). We set up improved radiative transfer calculations for scenes including aerosol particles (Gutleben et al., 2019) and ice clouds (Ewald et al., 2021; Röttenbacher et al., 2024) with the overall focus to achieve precise spaceborne radiative budget measurements that are consistent with corresponding radiative transfer simulations, which is one main goal of the EarthCARE mission. Furthermore, we used these synergistic EarthCARE-like measurements to prepare for the use and the validation of data collected by EarthCARE by investigating the impact of measurement sensitivity, wavelength combination, attenuation and instrument characteristics on the derived data products (Delanoë et al., 2020; Groß and Ewald, 2018). For that, we conducted dedicated HALO underflights with this payload closely coordinated CALIPSO and Cloudsat (Schäfler et al., 2018). Furthermore, we also used HALO together with the French SAFIRE Falcon and at a later stage ATR-42 as Tandem Platform (Delanoe et al., 2014). Our experiences supported the formulation of recommendations in a document for the best practices of validation for aerosol, cloud, and precipitation profiles (Amiridis et al., 2025).

These efforts culminated in the concept for PERCUSION (Persistent EarthCARE underflight studies of the ITCZ and organized convection) campaign (https://orcestra-campaign.org/percusion.html; last access 15 Jan. 2026), as a component of the campaign network ORCESTRA (Organized Convection and EarthCARE Studies over the Tropical Atlantic) (Stevens et al., 2025), combining different approaches for validation. In this work we give an overview of the PERCUSION campaign and the dataset's exploitation capability for the validation of EarthCARE, addressing the requirements and needs for EarthCARE validation (Section 2). The detailed description of the PERCUSION campaign with focus on validation includes information on instrumentation and measurement strategy (Section 3). In Section 4 we give an overview of the potential of PERCUSION for validation of the different EarthCARE instruments and different level products. Finally, we will conclude (Section 5) the work with a discussion of our findings and the potential for the use of the measured dataset, not only for EarthCARE but also for other satellite missions (e.g. the NASA PACE mission).

https://doi.org/10.5194/egusphere-2026-112
Preprint. Discussion started: 16 January 2026

2. Requirements for EarthCARE Validation

With the launch of the **Earth C**louds, **A**erosols and **R**adiation **E**xplorer (EarthCARE) satellite in May 2024, the most complex Earth Explorer Missions to date started to investigate aerosol particles and clouds, and their interactions and impacts on precipitation and the radiative energy budget (Wehr et al., 2023). EarthCARE is a joint mission of the European Space Agency (ESA) and the Japan Aerospace Exploration Agency (JAXA). It is equipped with a suite of four instruments together on one single platform. These include three instruments developed by ESA, the Atmospheric LIDar (ATLID), the Multi-Spectral Imager (MSI), and a BroadBand Radiometer (BBR), and the Cloud Profiling Radar (CPR) developed by JAXA and National Institute of Information and Communications Technology (NICT). The two active remote sensing instruments, the ATLID and the CPR, provide measurements of the vertical profiles of aerosol particle and cloud properties along the satellite track. The two passive remote sensing instruments, the MSI and the BBR, deliver the scene context information and radiation measurements. To quantify the measurement uncertainties and data product quality, a thoughtful and holistic validation is needed. A general approach for EarthCARE validation is given in the EarthCARE Scientific Validation Implementation Plan (VIP) of ESA (Koopmann, 2024), which is adapted and refined in the validation strategy of the EarthCARE Data Innovation and Science Cluster (DISC; ESA, 2024). This strategy includes also the outcome of a joint activity of the ESA EarthCARE Mission Advisory Group and instrument developers, which defines validation needs and target scenes of importance for EarthCARE validation (Hall, 2025). The aim is to provide information about the performance of EarthCARE data and retrievals in different synoptic regimes and for typical cloud and aerosol conditions.

2.1. Properties and Products

The EarthCARE data are categorized in level products (Table 1). The calibrated instrument data (Level 1b) for the three European instruments are provided by ESA, and for the CPR by JAXA. For higher level products, each Agency has its own processing chain. In this study we focus on the ESA processing chain. The data of the specific instruments are first processed individually (Level 1b and Level2a), and in a next step two or more instruments are processed in a synergistic way (Eisinger et al., 2024).

Table 1: EarthCARE Product Levels adopted from (Koopmann, 2024).

Level 0 Product	Raw instrument data, with duplicates removed and quality flags. For expert users only.
Level 1b Product	Instrument data processed to physical units, with error bars, quality flags and geolocations.
Level 1c Product	MSI only: Level 1b data re-sampled onto the grid of one selected MSI reference channel.
Level 1d Product	Auxiliary products.
Level 2 Product	Derived geophysical variables, with error bars, quality flags and geolocations.
Level 2a Product	Level 2 product derived from one single EarthCARE instrument
Level 2b Product	Level 2 product synergistically derived from two or more EarthCARE instruments

The ESA product chain generates 44 EarthCARE data products. They are introduced in detail by Eisinger et al. (2024) and the references therein. JAXA's Level 2 algorithms for EarthCARE from single instrument to four sensor synergistic retrievals are described by and the references therein. Besides the validation of the measurements (Level 1b) and the instrument data in

https://doi.org/10.5194/egusphere-2026-112
Preprint. Discussion started: 16 January 2026

geophysical unites (Level 2), specific needs for validation have been defined addressing the macro-physical properties as well as higher level products (ESA, 2023). They are briefly summarized in the following.

Table 2: Needs for EarthCARE validation adapted from the EarthCARE Mission Advisory Group and developers (ESA, 2023) to be addressed by PERCUSION measurements.

Uncertainty	Location/scene regimes	Instrument/Products
Macro-physical properties		
Aerosol layer detection and type classification	• Multi-layer aerosol scenes • Strong internal layering	ATLID and ATLID-MSI Target Classification
Aerosol/cloud discrimination	• Cloud embedded in aerosol layers	ATLID and ATLID-MSI Target classification and layer product
Cloud layer detection	• Multi-layer aerosol/cloud scenes • Cirrus cloud over liquid cloud • Non-precipitating liquid clouds	MSI, ATLID, CPR layer detection and target classification
CPR surface clutter removal	• Measurements over different surface types	CPR Feature Mask
Ice cloud and snow		
Snow microphysics	• Stratiform and convective systems	CPR cloud product and synergistic cloud retrieval
Ice microphysical properties	• Different cloud types with a variety of temperatures, locations	ATLID ice cloud product and synergistic cloud retrieval
Rain		
Melting layer structure and attenuation of CPR	• Heavy precipitation events • Convective and stratiform systems	CPR cloud products and synergistic cloud retrieval
Aerosol		
AOT over land and sensitivity to aerosol classification	• Different land surfaces • Different aerosol types	MSI aerosol optical thickness

2.2. Target Scenes

The aim of the target scene is to include validation activities which can provide information about the performance of EarthCARE data and retrievals in different synoptic regimes and for different cloud and aerosol conditions. They can be shortly summarized in the following:

- **Mixed aerosol types (MAT)**: To investigate the performance of ATLID under different aerosol conditions, types and concentrations and under different noise conditions (e.g. performance at daytime conditions compared to night-time conditions).
- **Cumulus and marine aerosol (CMA)**: Small scale, drizzle-free and often optically thin cumulus clouds are challenging to be characterized from satellite observations. They are hardly detectable by CPR, and it is important to accurately mask them for ATLID aerosol retrievals, especially of marine aerosols.
- **Marine stratocumulus (MSC)**: The detection of marine stratocumulus is challenging for satellite retrievals; the synergy of different EarthCARE instruments is thus key for their characterization. Drizzle-free clouds are barely detectable by CPR, and ATLID will be rapidly attenuated within the cloud. Measurements of the solar radiance in addition provide optical constrains. The evaluation of EarthCARE's performance to infer the location of marine stratocumulus, its cloud base and vertical extent and the profile of the liquid water path is thus important.

https://doi.org/10.5194/egusphere-2026-112
Preprint. Discussion started: 16 January 2026

- **Large-scale rain (LSR)**: To evaluate how accurate rain rates can be retrieved from CPR, large scale rain conditions have to be addressed in the comparisons. It affects the CPR measurements e.g. by attenuation due to rain.
- **Snow, including snow above the melting layer (SML)**: Snow and snow over ice are common features in mid-latitude weather systems and thus important for validation. Their multi-layer structure (e.g. also including embedded supercooled liquid layers) makes it challenging to properly detect and retrieve.
- **Cirrus (CC)**: Cirrus clouds are a main cloud type over large areas of the globe. They have a strong impact on the energy budget of the Earth with changing impact depending on optical and geometrical thickness. It is thus of importance to properly determine layer boundaries as well as optical and microphysical properties.
- **Complex multi-layer scenes (CLS)**: Multi-layer scenes are common in almost all synoptic regimes. A valid determination, separation and classification of the different layers are crucial to determine the overall radiative effect of the scenes. Combination of radar and lidar are often needed to determine different cloud types and to distinguish aerosols and clouds.
- **Deep convection (DC)**: Deep convection is challenging to properly investigate from satellite measurements. It consists of different cloud parts; cirrus outflow which is difficult to detect with radar, mixed-phase part which causes attenuation of the lidar and a precipitation part which might lead to attenuation even in the radar.

3. The HALO PERCUSION mission

PERCUSION (Persistent EarthCARE underflight studies of the ITCZ and organized convection) is an initiative of German research institutes and universities, which is led by the German Aerospace Centre DLR and by the Max-Planck-Institute for Meteorology. PERCUSION had two main objectives:

(1) To test factors hypothesized to influence the organization of deep maritime convection in the tropics and the influence of organized convection on the large-scale environment, and
(2) To establish confidence in EarthCARE by validating the EarthCARE measurements and data products.

Measurements with HALO with EarthCARE-like instrument payload were performed from August to November 2024. The EarthCARE readiness for correlative measurements was achieved just in time for PERCUSION, among others by adjusting initial calibration planning/sequencing, due to the expected importance of the campaign for EarthCARE validation during the commissioning phase and beyond.

3.1. HALO aircraft and instrumentation

HALO is a modified Gulfstream business jet G550. With a maximum cruising altitude of up to 15 km and a range of up to 10,000 km (~10 flight hours) it provides the capability for long and high flights and measurements over remote regions, which makes HALO ideally suited for satellite validation. During PERCUSION, the HALO aircraft was equipped as a flying cloud observatory (Stevens, et al., 2019) combining active and passive remote sensing instrumentations, i.e., a high spectral

https://doi.org/10.5194/egusphere-2026-112
Preprint. Discussion started: 16 January 2026

resolution and depolarization sensitive lidar system, and a cloud radar with doppler capability, together with imager and
175 radiation measurements (Table 3). In this configuration, HALO carries the most complete payload to mimic EarthCARE measurements. A large number of dropsondes (Stevens, et al., 2025) provided profiles of the meteorological context, and measurements taken by instrumentation installed in the nose boom setup of HALO complemented crucial information on high-resolution thermodynamic and dynamic (wind) parameters at flight altitude. Table 3provides a detailed summary of the HALO instrumentation and available products during the PERCUSION campaign.

https://doi.org/10.5194/egusphere-2026-112
Preprint. Discussion started: 16 January 2026

Table 3: Detailed information on HALO instrumentation during PERCUSION. Adapted from (Stevens et al., 2019).

Instrument	Institution	Observable	Derived products
HAMP (HALO Microwave Package) Radiometers (Mech et al., 2014)	MPI-M, University Hamburg, University of Cologne, DLR-PA	Brightness temperature at 26 selected microwave frequencies between 22 and 183 GHz	• Integrated Water vapor • Temperature + humidity
HAMP Doppler Cloud radar MIRA (Ewald et al., 2019)	DLR-PA, MPI-M, University Hamburg	Profiles of radar reflectivity, depolarization ratio & Doppler velocity	• Cloud, snow • Target classification • Cloud geometry
WALES (Water vapor lider experiment in space) (Wirth et al., 2009)	DLR-PA	Profiles of • Atmospheric backscatter ratio at 532 nm, 935 nm and 1064 nm • Particle linear depolarization ratio at 532 nm • Particle extinction coefficient at 532 nm	Profiles of • Water vapor mixing ratio • Cloud mask • Aerosol classification • Extinction-to-backscatter ratio
specMACS (spectrometer of the Munich Aerosol Cloud Scanner) (Ewald et al., 2016; Weber et al., 2024)	LMU München	• Upward spectral radiance (400 – 2500 nm) with across-track field-of-view of 35° at a sampling rate of 30 Hz • Polarized radiance at RGB color channels, 2D fields (91° x 220°) at 5Hz sampling rate	• Cloud mask • Cloud phase • Cloud optical thickness • Effective particle size • Particle size distribution
BACARDI (Broadband AirCrAft RaDiometer Instrumentation) (Ehrlich et al., 2023)	Leipzig University	Upward and downward broadband irradiances • solar (0.3 -3 µm) • thermal-infrared (3-100 µm)	• Radiative energy budget • Cloud radiative effect • Heating and cooling rates
SMART (Spectral Modular Airborne Radiation Measurement System (Wendisch et al., 2001; Wolf et al., 2020)	Leipzig University	• Spectral upward and downward irradiance (300-2200 nm) • Spectral upward radiance (300-2200 nm)	• Spectral solar radiative energy budget • Cloud optical thickness • Liquid water path, effective particle size • Cloud thermodynamic phase
VELOX (Video airbornE Longwave Observations within siX channels) (Schäfer et al., 2022)	Leipzig University	Two dimensional fields of brightness temperature in 6 channels between 7.7 µm and 12.0 µm with 100 Hz temporal and 640 x 512 pixel resolution (field-of-view of 35.5° x 28.7°)	• Cloud mask, phase • Cloud top temperature • Cloud top altitude • Surface temperature
Dropsondes	MPI-M, DLR-PA, University Hamburg	Profiles of • Relative humidity • Temperature • Horizontal wind	
BAHAMAS (Basic Halo Measurement and Sensor System) (Giez et al., 2023)	DLR-FX	In-situ observations of T, q, u, v, w, 100 Hz data navigational data, GPS, flight attitude	

3.2. Data analysis

In addition to setting up an airborne EarthCARE-like payload on HALO to prepare for validation, we developed independent

https://doi.org/10.5194/egusphere-2026-112
Preprint. Discussion started: 16 January 2026

retrievals to derive similar data products as those from EarthCARE. This includes a lidar based aerosol classification (Groß et al., 2013; Groß et al., 2015) that was extended to include cloud radar measurements for a full target classification (Marinou, et al., 2020), as well as a method to derive cloud and aerosol layer heights and area (Groß et al., 2014; Dekoutsidis et al., 2023; Gutleben et al., 2019). The airborne radar is calibrated (Ewald et al., 2019) and the measurements are analysed. Subsequent of the basic analysis of both active remote sensing measurements, the data are used in a variational retrieval (Delanoë and Hogan, 2008; Cazenave et al., 2019) to derive higher level products; e.g., ice water content and ice effective radius. This retrieval was further developed to consider mixed-phase clouds and layers of super-cooled water (Aubry et al., 2024). Aerosol and cloud optical and microphysical properties are used to calculate their radiative properties, e.g., heating rate profiles, top of the atmosphere radiances, and spectral radiance of clouds using the library for radiative transfer – libRadtran (Mayer and Kylling, 2005; Emde et al., 2016; Gutleben et al., 2020; Ewald et al., 2021), which can be directly compared to spectral radiance measured onboard HALO (Ewald et al., 2021) or to radiation measurements provided by EarthCARE. specMACS data are used to determine cloud top height and geometry using a stereographic algorithm Next to the general analysis of the specMACS system (Weber et al., 2024) cloud top height can be derived from a stereographic algorithm to determine cloud geometry (Kölling et al., 2019, Volkmer et al., 2024). Cloud phase (Ehrlich et al., 2008; Weber et al., 2025) and cloud droplet radius (Pörtge et al., 2023) are determined with high accuracy and high spatial resolution from the polarimetric angular observations. The thermal-infrared imager VELOX and the broadband radiometer BACARDI are radiometrically and geometrically calibrated as described in detail by Ehrlich et al. (2023) and Schäfer et al. (2022). Atmospheric corrections based on radiative transfer simulations using the radiosonde measurements and the EarthCARE auxiliary data products are applied to the VELOX and BACARDI measurements. These corrections adjust the measurements in HALO flight level to top-of-atmosphere (TOA) brightness temperatures and broadband radiative fluxes comparable to MSI and BBR observations.

Using the HALO measurements, we can address many of the validation needs for EarthCARE measurements and data products.

https://doi.org/10.5194/egusphere-2026-112
Preprint. Discussion started: 16 January 2026

Table 4 gives an overview of the EarthCARE in-orbit data products that can be validated with the PERCUSION measurements.

Table 4: EarthCARE in-orbit data products addressed for validation by PERCUSION

Earth CARE Products	
Level 1	MSI*
	ATLID
	CPR
Target classification	Cloud-top height
	Cloud-top phase
	Aerosol layer height/depth
	Aerosol layer classification
	Cloud detection, Cloud aerosol discrimination
	Cloud/precipitation fraction
	Cloud/precipitation phase
	Aerosol fraction
	Aerosol species
Ice cloud & snow	Optical thickness
	Effective radius
	Water path
	Extinction
	Extinction-to-backscatter ratio
Aerosol (per species)	Aerosol optical thickness
	Aerosol extinction
	Extinction-to-backscatter ratio
	Particle linear depolarization ratio
Radiation	BBR-SW unfiltered radiances
	Solar top-of-atmosphere flux
	Terrestrial top-of-atmosphere flux

*The Across-Track Radiances could be provided by specMACS as Push-Broom Scanner. However, only the NADIR FOV of the BBR but not the AFT/FRONT FOVs can be compared. VELOX images can be merged along the flight track to create push-broom like images. Therefore, across-track radiances can be provided as well in the thermal-infrared.

3.3. Measurement strategy

To achieve the objectives of PERCUSION, measurements were performed out of three different locations (Figure 1):

- **Sub-tropical and tropical Atlantic East (Sal, Cape Verde)**: From 8 August to 5 September 2024 HALO flights were carried out of Sal (Cape Verde). This period provided the possibility for coordination with the French EarthCARE airborne validation activity within the MAESTRO (Mesoscale organisation of tropical convection) campaign and with validation activities of the Norwegian-Romanian validation activities (CELLO; Cloud and EarthCARE caL/vaL Observations), as well as with ground-based ACTRIS (The Aerosol, Clouds and Trace Gases Research Infrastructure) validation measurements from TROPOS at Minedlo (CLARINET; CLoud and Aerosol Remote sensing for EarThcare), and with shipborne measurements onboard the German Research Vessel (RV) Meteor (BOWTIE; Beobachtung von Ozean und Wolken – Das Trans ITCZ Experiment (Klocke et al., 2025)).
- **Sub-tropical and tropical Atlantic West (Barbados):** Following the measurements from Cape Verde, HALO was transferred to Barbados to perform measurement flights over the western (sub-)tropical Atlantic until End of

https://doi.org/10.5194/egusphere-2026-112
Preprint. Discussion started: 16 January 2026

September 2024. During this part of the mission, the measurements were linked to ground-based measurements from the Barbados Cloud Observatory (BCO; Stevens, et al., 2016) on Barbados and to measurements onboard RV Meteor.

- **Mid- and high-latitudes (Oberpfaffenhofen, Germany):** After a small break, additional validation flights were performed out of Oberpfaffenhofen, the homebase of HALO, from 4 to 19 November 2024. During this part of the validation campaign, it was aimed to coordinate with ground-based stations in Germany and Greece taking part in EarthCARE validation activities.

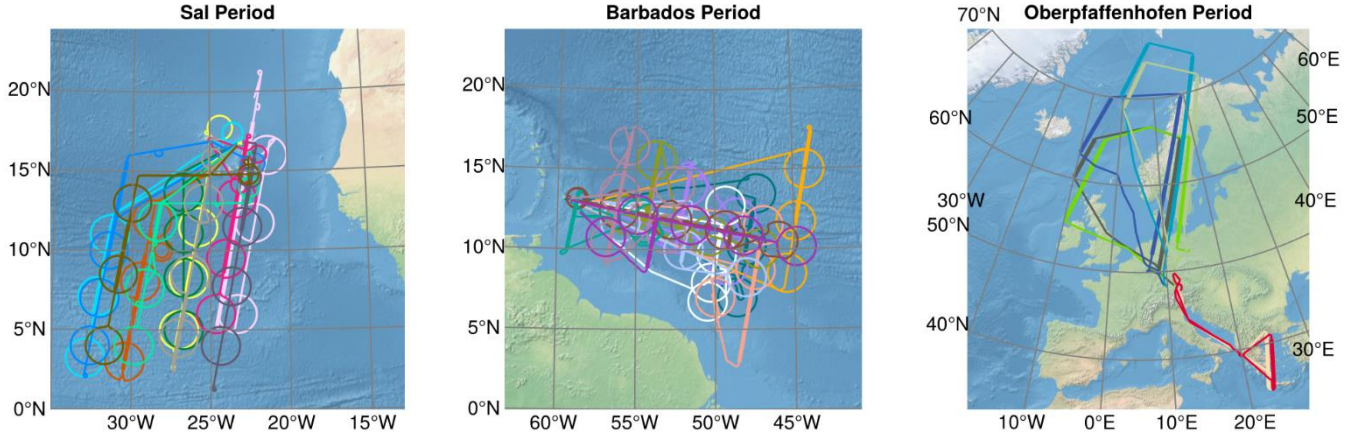

Figure 1: Flight tracks of the HALO research aircraft during the PERCUSION campaign out of Sal (left), Barbados (middle) and Oberpfaffenhofen (right). The straight thick lines indicate direct underpasses under the EarthCARE satellite.

The flights were planned in a way that at least one EarthCARE underpass was included in every flight; for direct comparisons, but also to put EarthCARE measurements in the centre of the scientific studies. During the southern part of PERCUSION with flights out of Sal and Barbados, the EarthCARE track guided the position of the HALO flights. The HALO flight plan followed the EarthCARE track either in northern or southern direction to capture once the whole atmospheric condition. The direct underpass was included in these straight flight legs varying from day to day in time and location to capture different aerosol and cloud conditions and to coordinate with other measurements platforms. For comparability of the EarthCARE and HALO measurements, we anticipated to be at least about 10 minutes before and 10 minutes after the direct overpass on the EarthCARE track. In addition to the straight flight legs on the EarthCARE tracks we included circles in the flight plan to investigate vertical motions (Bony and Stevens, 2019). Flights out of Cape Verde and Barbados were conducted during daytime. Considering an EarthCARE equator crossing time around 14:00 local time, this results in an underpass time around 14:30-16:30 local time (see Table 5). Information on flight plans, measurement situation and performance of each flight can be found at https://orcestra-campaign.org/operation/halo.html. During the third part of PERCUSION, out of Oberpfaffenhofen, we solely aimed for EarthCARE validation. Flights were either planned in northern direction capturing continental conditions, cirrus clouds, and frontal cloud systems, and high-latitude regions with measurements in night-time conditions, or they were planned to measure in Mediterranean conditions with flights over the Greek ground-stations in Antikythera and Thessaloniki. During the northern flights we catched EarthCARE twice, one in northern direction and once in southern direction of HALO. The time

https://doi.org/10.5194/egusphere-2026-112
Preprint. Discussion started: 16 January 2026

of the meeting point with EarthCARE was at around 15:00 and 17:00 local time. Underpasses in the northern parts of the flight track were thus performed already in nighttime conditions. In all the flights we included overpasses over ground-stations whenever possible.

3.4. Meeting EarthCARE

Essential for the validation of satellite data by airborne measurements is a precise local and time match of the airborne and the spaceborne measurements to ensure that the airborne systems and the satellite systems are sampling the same airmasses. Table 5 summarizes information on co-location of HALO with EarthCARE during PERCUSION. PERCUSION took place very early after the launch of EarthCARE. This is why the satellite was still in a drifting phase, hence the prediction of the EarthCARE track was not as precise and thus underflights were challenging. We adapted the flight path of HALO just before or partly even during the flight to the latest predictions and therefore managed to capture EarthCARE with a distance of less than 500 m except for the two first flights, where we had a distance of about 1000 m, which is still sufficient for validation and most of the time within the CPR footprint on ground of 750 m. The ATLID has a footprint of 15 m on the ground. Another aspect is, that due to the slower flight speed of HALO, a perfect temporal collocation is only achieved at the rendezvous location. Depending on the across-track winds, cloud fields may move out of the satellite swath while HALO is sampling the scene. Similar convective clouds may develop in short time. The alignment of HALO along the EarthCARE track was maintained mostly 15 min before and 15 min after the overpass of Earth CARE to minimize this effect, still, these potential shifts need be taken into account during the validation.

In addition to the detailed information on the meeting point with EarthCARE, Table 3 also includes information on the scene that was targeted for comparison on the individual days. The table shows that all target scenes that have been identified as important (Section 2.2) for a full validation could be captured during PERCUSION. Even a snow case could be captured during one of the northern, homebased flights.

https://doi.org/10.5194/egusphere-2026-112
Preprint. Discussion started: 16 January 2026

Table 5: Detailed information about EarthCARE underpasses including date of the flight, HALO base, underflown EarthCARE orbit, start time and end time on EarthCARE track (UTC), best match time (UTC), distance and location (lon/lat), and scene targeted for comparison.

Date	Base	Orbit	Time on EC track	Best match	Match dist.	Lon. °E	Lat. °N	Target Scenes
11 Aug.	Sal	01162E	15:22:37 – 16:09:11	15:52:02.743	996 m	-26.5562	17.1985	CC, CMA
13 Aug.	Sal	01193E	15:32:50 – 17:13:34	15:40:00.326	1090 m	-22.3079	17.1985	MAT
16 Aug.	Sal	01240E	16:03:18 – 16:51:28	16:14:04.527	441 m	-32.1054	7.3831	CLS, CC
18 Aug.	Sal	01271E	15:30:00 – 16:28:00	16:04:07.527	336 m	-29.7063	6.7818	CLS, CC
22 Aug.	Sal	01333E	14:57:00 – 16:04:00	15:41:22.111	131 m	-23.1087	14.1737	DC, LSR
25 Aug.	Sal	01380E	15:40:00 – 16:35:00	16:11:49.766	84 m	-30.9127	12.8612	MAT
27 Aug.	Sal	01411E	15:57:00 – 16:17:00	16:01:17.237	249 m	-26.9773	4.8126	MAT, CLS
29 Aug.	Sal	01442E	15:34:00 – 16:12:00	15:51:57.580	185 m	-22.6153	13.2611	DC, LSR
31 Aug.	Sal	01473E	15:24:00 – 16:00:00	15:38:41.850	253 m	-22.6153	13.2611	MAT
3 Sept.	Sal	01520E	16:00:00 – 16:34:00	16:09:04.874	22 m	-30.8138	8.6363	DC, LSR
7 Sept.	Barbados	01583E	17:10:00 – 17:39:00	17:18:30.109	192 m	-47.9594	10.4881	CLS
9 Sept.	Barbados	01614E	16:28:00 – 17:19:00	17:05:43.005	419 m	-44.1018	15.7095	MLS, CMA
12 Sept.	Barbados		17:10:00 – 17:53:00	17:35:33.811	30 m	-52.0739	12.1760	CMA
14 Sept.	Barbados	01692E	17:13:24 – 17:38:21	17:25:38.715	427 m	-49.8648	9.8595	CMA
16 Sept.	Barbados	01723E	16:52:00 – 17:51:00	17:16:06.878	384 m	-47.9917	5.8568	CMA, MSC
19 Sept.	Barbados	01770E	17:28:50 – 18:04:40	17:43:56.788	31 m	-53.8761	14.5050	CC, CMA
21 Sept.	Barbados	01801E	17:19:20 – 17:47:00	17:33:48.109	340 m	-51.7980	11.0166	CMA
23 Sept.	Barbados	01832E	17:14:00 – 17:24:00	17:22:33.535	330 m	-48.9818	11.1494	CC
24 Sept.	Barbados	01848E	17:48:00 – 18:17:40	18:03:00.027	298 m	-59.0219	11.7467	CC
26 Sept.	Barbados	01879E	17:20:40 – 18:21:00	17:51:55.041	291 m	-56.0327	13.5465	CLS, CMA
28 Sept.	Barbados	01910E	17:31:06 – 17:54:38	17:42:05.368	345 m	-53.9846	10.4329	CC, CMA
5 Nov.	Oberpf.	02499D	11:57:23 – 13:59:4	13:55:33.786	446 m	15.9275	64.3926	CC
		02500 D	15:26:03 – 16:07:26	15:28:00.709	475 m	-6.9707	64.7040	MSC, MAT
7 Nov.	Oberpf.	02530D	12:02:00 – 13:46:22	13:44:34.029	302 m	18.8376	64.6444	CLS, MSC
		02531D	15:16:19 – 16:48:19	15:17:02.613	309 m	-4.0945	64.9118	CC, MSC
10 Nov.	Oberpf.	02576D	12:15:04 13:02:30	12:48:48.217	226 m	23.0967	36.9121	CMA, CC
12 Nov.	Oberpf.	02608C/D	11:10:00 14:04:50	14:01:15.588	246 m	18.6452	69.3839	CC
		02609C/D	15:17:43 16:21:25	15:34:07.741	397 m	-5.7937	68.1341	CLS, SML
14 Nov.	Oberpf.	02639C/D	11:04:09 14:01:47	13:49:39.396	242 m	25.1685	72.3513	MLS, MSC
		02640C/D	14:47:13 15:38:00	15:22:16.125	296 m	1.7593	72.1700	CC
16 Nov	Oberpf.	02670C/D	11:47:09 13:58:49	13:39:50.884	329 m	23.8375	69.2438	DC, LSC
		02671C/D	14:52:16 15:36:22	15:11:40.927	426 m	3.9543	71.8482	CC, CMA
19 Nov.	Oberpf.	02716D	12:10:12 12:52:47	12:46:04.513	27 m	23.5290	35.8059	MAT, CMA

https://doi.org/10.5194/egusphere-2026-112
Preprint. Discussion started: 16 January 2026

4. PERCUSION's potential for EarthCARE Validation

In the following we will give an overview, of how the HALO measurements with an EarthCARE-like payload can be used for the validation of the EarthCARE measurements and data products. The validation examples presented here are limited to individual EarthCARE overpasses. Depending on the specific focus of the validation, flights over the tropics or high-latitude observations were chosen. A statistical comparison of all PERCUSION flights quantifying EarthCARE performance in a more general way will be done in future studies. A more detailed information on the validation findings of the different products will be given in specific validation studies. In this paper we focus on the demonstration of the direct comparability of the measurements. Cross-validation is also of importance and will be done in dedicated studies, but is not in the scope of this work.

4.1. Atmospheric Lidar (ATLID)

WALES-ATLID comparison for L1 and L2 optical properties

The lidar system WALES is an airborne water vapor differential absorption and high spectral resolution lidar (HSRL) developed and built at DLR (Wirth et al., 2009). It measures the water vapor field along the flight track from cruise altitude to ground with four wavelengths around 935 nm, and the extinction using the HSRL technique at 532 nm deploying an iodine filter. In addition, it is equipped with polarization sensitive measurements. The raw data resolution is 0.2 s and 15 m in height. The data are typically provided horizontally integrated over 1 s for the aerosol and cloud measurements and over 25 s for the water vapor data. To demonstrate the potential of WALES to validate ATLID-L1b (EarthCARE ATLID NOM Level 1B) and L2 (EarthCARE ATLID EBD Level 2A) optical properties (baseline BA) derived from A-PRO algorithm (Donovan et al., 2024), we focus on a research flight out of Sal on 13 August 2024, to compare ATLID aerosol measurements and products for orbit 01162E. In this case of Saharan dust. Looking at the time-height cross section of the backscatter coefficient of both lidar instruments (Figure 2) we can identify an aerosol layer up to about 4 to 5 km altitude. In the ATLID measurements we see enhanced backscattering at around 15 km altitude missed by the WALES measurements due to the lower flight altitude of HALO of about 11 km. In addition to the aerosol layer that is visible well in the measurements of both systems, we can identify signatures of low clouds from about 0.5 km to about 2 km.

https://doi.org/10.5194/egusphere-2026-112
Preprint. Discussion started: 16 January 2026

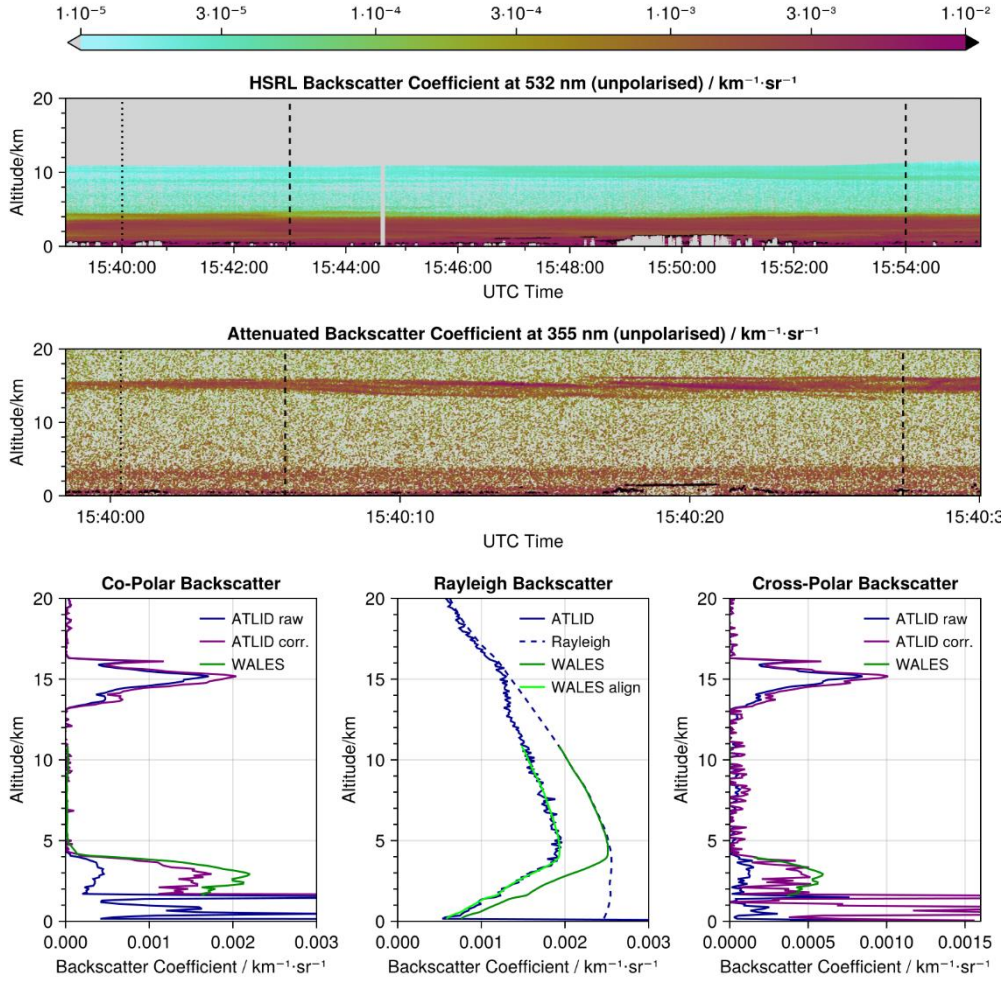

Figure 2: Comparison of the WALES HSRL Backscatter Coefficient at 532 nm (upper panel) and ATLID Attenuated Backscatter Coefficient at 355 nm (lower panel) for an underflight performed on 13 August 2024 out of Cape Verde. The dotted line shows the position of closest match. The dashed vertical lines mark the 120 km length region for the comparison of the co-polar backscatter profile, Rayleigh backscatter profile and cross-polar backscatter profile. The left lower panel shows the mean profiles of the backscatter coefficient for co-polar polarization for WALES (green) and for ATLID without extinction correction (blue) and in with extinction correction (purple). The middle lower panel shows the Rayleigh backscatter from ATLID (solid blue line), the expected pure Rayleigh backscatter signal calculated from an atmospheric density profile (dashed blue line) and the pure Rayleigh signal at 355 nm with additional aerosol extinction derived from the WALES measurements (dark green line). The light green line is aligned to the ATLID profile at the uppermost point of the WALES profile. The right lower panel shows the mean profiles of the backscatter coefficient for cross-polar polarization for WALES (green) and for ATLID without extinction correction (blue) and with extinction correction (purple).

To validate ATLID L1 (A-NOM) products, we directly compare the profiles of the measured Mie backscatter coefficient, Rayleigh backscatter coefficient, and Cross-polar backscatter coefficient. As the measurement situation is stable (see Figure 2) for comparisons of the co-polar Backscatter profile, Rayleigh backscatter profile and cross-polar backscatter profile a region of 120 km length with homogenous backscatter close to the overpass point is selected to increase the signal-to-noise ratio (SNR) of ATLID data for the comparison. For the direct comparison of L1 data we have to take into account, that ATLID and

https://doi.org/10.5194/egusphere-2026-112
Preprint. Discussion started: 16 January 2026

WALES are operated at different wavelengths, i.e. 355 nm and 532 nm, respectively. The backscatter coefficient for co-polar polarization for WALES and for ATLID is compared without extinction correction and with extinction correction as is the case for the WALES profile. For evaluating of the ATLID Rayleigh backscatter, we take into account the expected pure Rayleigh backscatter signal calculated from an atmospheric density profile and the pure Rayleigh signal at 355 nm with additional aerosol extinction derived from the WALES measurements. We aligned the ATLID profile at the uppermost point of the WALES profile. The benefit of the general same measurement technique allows to address issues like cross-talk and background corrections. For the current baseline version (BA) of ATLID L1 data we can confirm a general good quality of the ATLID Mie and Rayleigh backscatter coefficient.

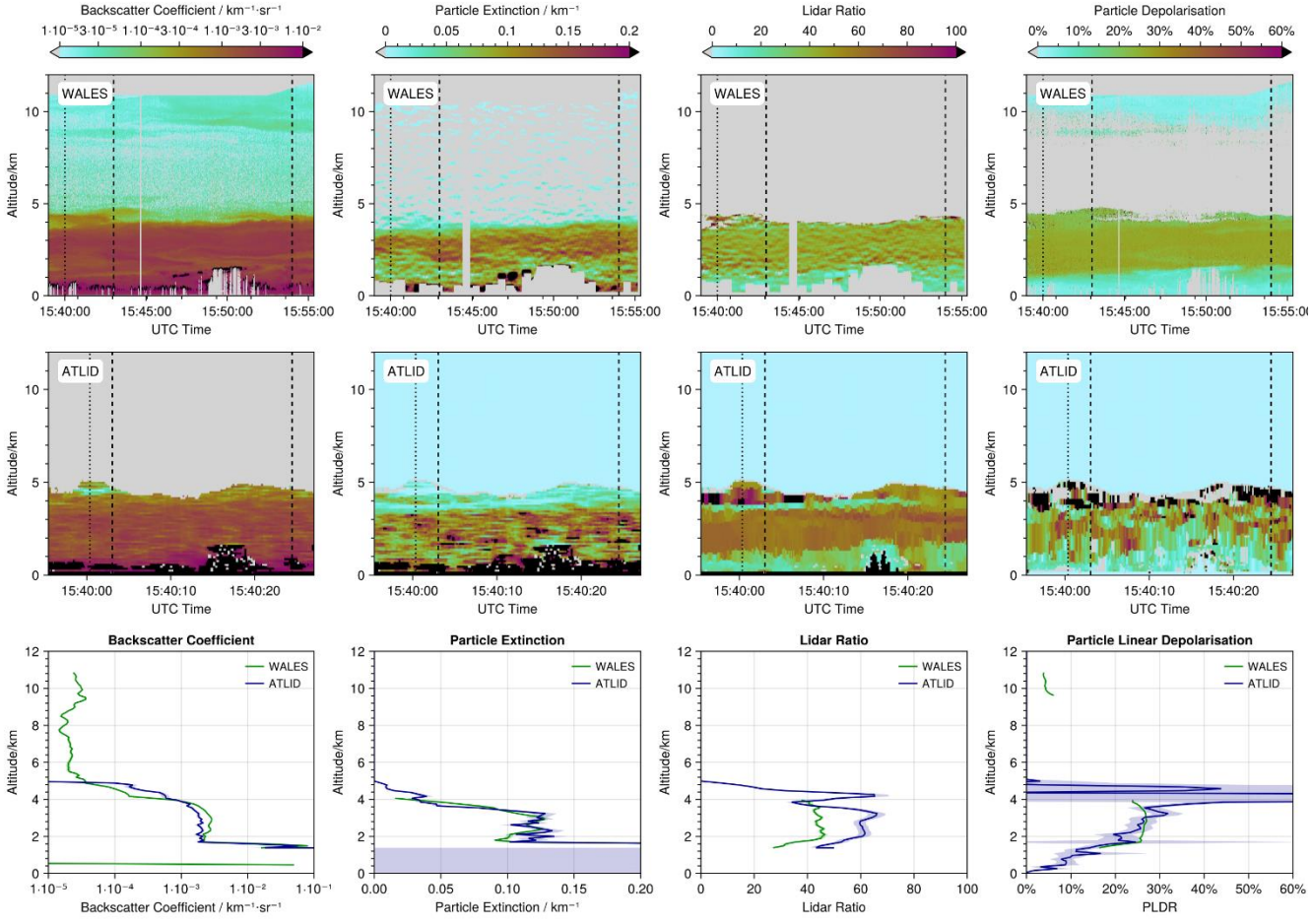

Figure 3: Time-height cross-section of the WALES optical properties (upper panel), and the ATLID optical properties (mid panel), and the profile comparisons (lower panel) of the backscatter coefficient (left), extinction coefficient (middle left), the lidar ratio (middle right), and the particle linear depolarization ratio (right) during the EarthCARE underpass on the 13 August 2013. The profiles are averaged within ±50 km around the EarthCARE overpass, indicated by the left and right vertical lines in the time-height cross-sections.

https://doi.org/10.5194/egusphere-2026-112
Preprint. Discussion started: 16 January 2026

After confirming the good performance of the Level 1b data, we investigate the quality of the ATLID L2a products of the cloud and aerosol profile processor (A-PRO (Donovan et al., 2024), including the A-AER aerosol product, and the A-EBD extinction, backscatter, and depolarization product (A-EBD), the A-TC target classification product, and the A-ICE ice microphysical estimation product. For the given example shown in Figure 2 we present as an example the comparisons of WALES optical properties and A-EBD products, i.e., the extinction coefficient, the backscatter coefficient, the lidar ratio and the particle linear depolarization ratio (Figure 3). For the validation analysis we use the latest available baseline version BA. Again, we have to consider a possible wavelength dependence, but former studies (e.g. Groß et al., 2011) confirm, that Saharan dust and marine aerosol layers do not show a wavelength dependence between 355 nm and 532 nm for the backscatter coefficient, extinction coefficient, and for the lidar ratio. For the particle linear depolarization ratio of Saharan dust, a small wavelength dependence between 355 nm and 532 nm is expected but well characterized (Freudenthaler et al., 2009; Groß et al., 2011; Groß et al., 2015; Groß et al., 2025; Burton et al., 2016; Haarig et al., 2022). Early comparisons have identified issues in the layering of the A-EBD properties that could be solved in the current baseline. From comparisons with the HALO measurements, we could clearly identify the problems that could be solved in the updated baseline BA of the products. Our comparisons confirm the good quality of the A-PRO products in the current baseline version. In the example shown above, significant noise on the depolarization values is observed in the top of the dust layer.

WALES-ATLID-L2 comparison

Besides the L2 optical properties we compare the WALES measurements to the ATLID Target Classification (EarthCARE ATLID TC Level 2A) and Feature Mask (EarthCARE ATLID FM Level 2A) (Donovan, et al., 2024) and layer properties. In this example, the ATLID cloud top height (EarthCARE ATLID CTH Level 2A) (Wandinger et al., 2023) (baseline BA) is compared to WALES measurement for the underflight on 16 August 2024 southwest of Cabo Verde (orbit 01240E. This flight was selected as it exhibits a wide range of cloud features and aerosol conditions representative of the tropical atmosphere. The flight objective aimed at a north-south-north transect across the ITCZ, including a flight leg of about 700 km (50 minutes) flown along the predicted EarthCARE ground track, extending from the ITCZ centre toward its northern edge. Figure 4a shows a time-altitude cross section of the backscatter ratio (BSR) measured with the WALES instrument along the EarthCARE leg (with the satellite underpass at 16:14 UTC). The vertical distribution of BSR illustrates the occurrence of various cloud types and aerosol layers encountered throughout this flight section: At the highest altitudes (10-13 km) the frequently high BSR values indicate a widespread field of ice clouds which has the largest vertical extent near the underpass and is more patchy and vertically thin in the northern part. At lower altitudes (1–3 km), isolated and smaller-scale patches of elevated BSR values (> 20) are detected, associated with stratocumulus and cumulus (liquid) cloud formations. Furthermore, within the lowest 6 km of the atmosphere, a vertically extended layer characterized by moderate BSR values (BSR between 2-6) indicative of a marked aerosol layer. Notably, this aerosol layer appears thicker and more continuous in the northern segment (track distance > 400 km) of the flight leg, whereas in the southern segment it is fragmented into two distinct layers— an elevated layer near 5 km altitude and another covering the lowermost 2 km of the atmosphere. Threshold-based detection algorithms are applied for

https://doi.org/10.5194/egusphere-2026-112
Preprint. Discussion started: 16 January 2026

determining a target classification (Groß et al., 2013; Marinou et al., 2019). In this example, however, the focus is exclusively on the validation of EarthCARE cloud products. In particular, we focus on cloud macro-physical properties from the target classification product (A-TC) providing information on the vertical distribution of clouds and the cloud top height product (A-CTH). To validate both products, cloud pixels and the altitude of the uppermost cloud are determined from the WALES BSR data set based on a height-dependent threshold-based algorithm as used in previous studies (e.g. Groß et al., 2014; Gutleben et al., 2019; Dekoutsidis et al., 2023; Urbanek et al., 2017).

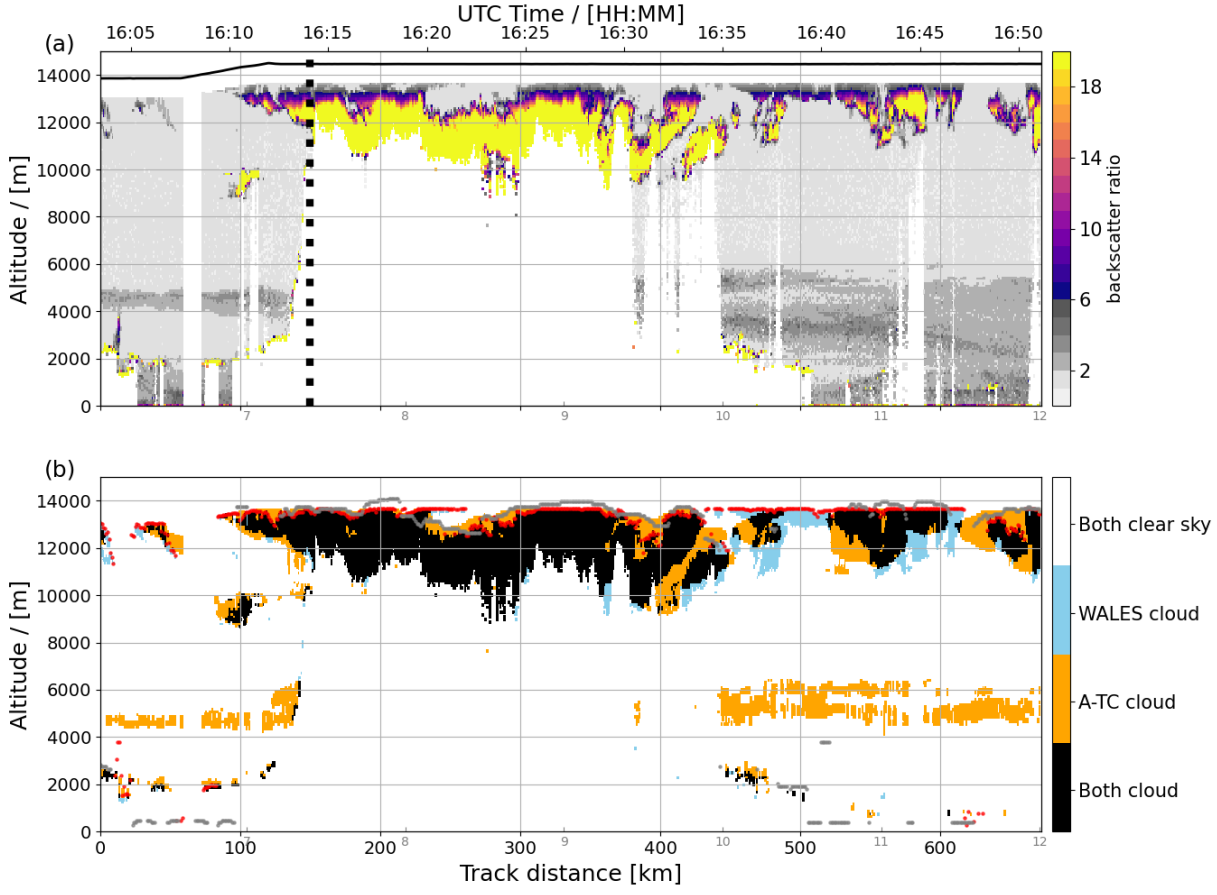

Figure 4: Distance-altitude cross sections for the HALO flight on 16 August 2024 showing a) the backscatter ratio measured with the WALES HSRL (contours), along with the flight altitude of the HALO aircraft (black solid line) and the EarthCARE underpass track (thick black dashed line). Panel b) displays the combined cloud mask derived from the WALES BSR data and the collocated EarthCARE L2 target classification product (A-TC). Black contours indicate cloud pixels detected by both WALES and A-TC, while blue and orange colors represent cloud pixels identified exclusively by WALES or A-TC, respectively. White denotes regions with no cloud detection by either product. The dotted lines in panel (b) correspond to the top altitude of the highest cloud layer detected from the WALES backscatter ratio and the cloud top height provided by the A-CTH product.

Figure 4b shows the cross section of the combined cloud mask from WALES BSR and A-TC to directly compare both products along the coordinated EarthCARE underflight. The black shaded areas indicate a strong agreement in the vertical distribution

https://doi.org/10.5194/egusphere-2026-112
Preprint. Discussion started: 16 January 2026

of cloud pixels in both cloud masks, especially for high-altitude cirrus clouds and for the cumulus cloud formations at altitudes between 1 and 3 km. Interestingly, A-TC-only pixels (orange), associated with both cirrus and cumulus clouds, indicate comparatively thicker vertical clouds. Cirrus clouds in particular are more horizontally spread, and thus less patchy in the A-TC cloud mask. The tendentially vertically thicker cirrus clouds in the A-TC correspond to the elevated cloud tops (red line) of the A-CTH product. Furthermore, it is noted that the A-TC-only mask shows a coherent cloud structure at an altitude between 4 and 6 km, which corresponds exactly to the upper part of the aerosol layer (Figure 4a) suggesting a misclassification of cloud and aerosols in this scene. The BSR measurements illustrate that the WALES-BSR dataset can be reliably used to determine macro-physical cloud properties (e.g., vertical distribution, horizontal and vertical extent, and cloud top information), and to validate the ATLID level 2 relevant products. The case study presented indicates that the A-TC product reliably represents all cloud features observed by WALES (extended high-altitude clouds and low-altitude clouds). There are indications that the cloud pixels in A-TC, especially ice clouds, are too large horizontally and vertically, which could be due to "bad layering" in the product algorithms. There are also indications that the cloud tops of the independent A-CTH product are higher than those derived from WALES and, in some cases, inconsistent with the cloud mask of A-TC.

4.2. Cloud Profiling Radar (CPR)

The CPR onboard HALO is a high-power (30 kW peak) magnetron-based MIRA35 cloud radar at 35.2 GHz manufactured from METEK. It has been thoroughly characterized and calibrated (Ewald et al., 2019). With a repetition rate of 7.5 kHz, the minimum detectable signal at 10 km (1s avg) is around -42 dBZ and thus at least 6 dB higher compared to CPR. Including effects of platform motion and natural spectral width, the effective sensitivity is around -34 dBZ. The vertical resolution of the MIRA35 measurements is significantly finer (30 m vs 500 m), and the horizontal resolution is twice as high (200 m vs 500 m) compared to CPR. Due to the lower frequency (35 vs 94 GHz), the gaseous and hydrometeor attenuation is also considerably lower for MIRA35 observations. Figure 5 shows the comparisons between space- and airborne measurements of the radar reflectivity (Figure 5a, b) and doppler velocity (Figure 5c, d) performed on the 18 August 2024 (orbit 01271E). The

https://doi.org/10.5194/egusphere-2026-112
Preprint. Discussion started: 16 January 2026

measurements were performed in the Tropical Atlantic roughly 1500 km south-east from Cape Verde above a convective region within the ITCZ.

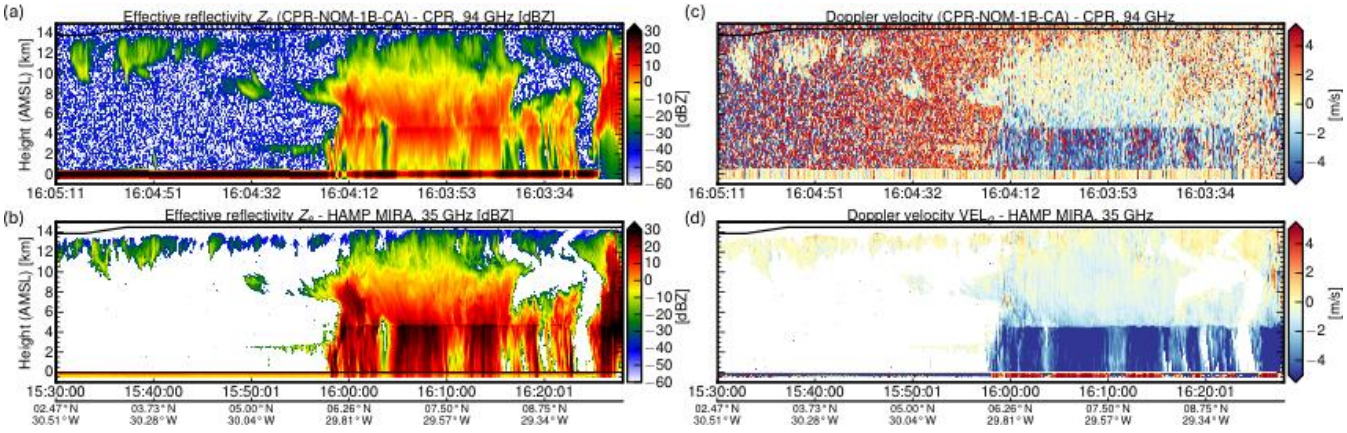

Figure 5: Comparison of (a) CPR and (b) MIRA radar reflectivity and of the doppler velocity from (c) CPR and (d) MIRA for a HALO underpass of Earth CARE performed on 18 August 2024.

Between the measured radar reflectivity from MIRA (Figure 5b) and CPR (Figure 5a), the coarser resolution and slightly lower sensitivity of CPR is most apparent for the thin cirrus at cloud top. Moreover, the different Mie scattering regime and the different absorption by hydrometeors stands out in the rain region below the melting layer. As this measurement was acquired during the commissioning phase, the redundant signal processing unit (SPU-A) of CPR was used which exhibited an IQ offset and a reduced signal sensitivity. This increased the noise in doppler measurements (Figure 5c) and caused the rainbow-like pattern in the clear-sky region. Figure 6 compares the mean profiles of radar reflectivity (Figure 6a, NOM-1B-CA) and doppler velocity (Figure 6b, CD-2A-AC) in absolute numbers. In the cloud top region between 6-10 km with negligible gaseous and hydrometeor attenuation and predominant Rayleigh scattering, the radar reflectivity bias was initially quite negative (-3.8 dB) for the early processing baseline BA. The bias improved to -1.6 dB for baseline CA until it was resolved for baseline CB. For the level 2 doppler velocity product CD-2A, the antenna miss-pointing correction by Puigdomènech Treserras et al. (2025) successful removed any velocity biases. Below an altitude of 6 km, the radar reflectivity mainly differs due to the differential hydrometeor attenuation between 35 GHz and 94 GHz. The difference in the mean doppler velocity can be explained by Mie scattering at 94 GHz of larger and faster falling rain droplets, underrepresenting their faster velocity component in the mean doppler velocity.

https://doi.org/10.5194/egusphere-2026-112
Preprint. Discussion started: 16 January 2026

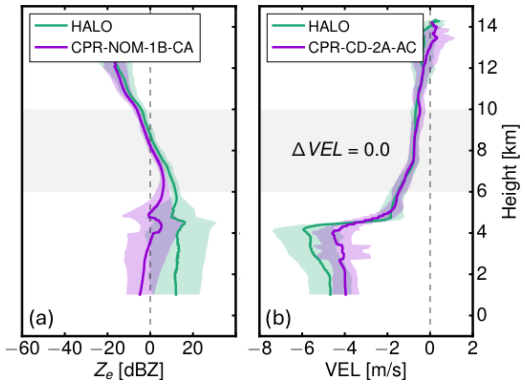

Figure 6 Comparison of mean observed profiles between HALO and EarthCARE (a) Radar reflecitivtyL1 product CPR-NOM-1B-CA and (b) L2 product CPR-CD-2A-AC for the underflight shown in Figure 5.

4.3. Multi Spectral Imager (MSI)

4.3.1 Comparison specMACS-MSI

specMACS consists of two hyperspectral line cameras (Ewaldet al., 2016) covering the visible and near-infrared (VNIR, 400 - 1000 nm) and the short-wave infrared (SWIR, 1000 - 2500 nm), as well as four 2D polarization resolving RGB cameras (Weber et al., 2024), providing an across-track field of view of about 220°. The VNIR and SWIR measurements during the 33 EarthCARE underflights of the PERCUSION campaign allow a direct comparison of the measured reflected radiances to the ones measured by the four MSI channels with center wavelengths at 670 nm and 865 nm in the VNIR and 1650 nm and 2210 nm in the SWIR, respectively. An exact validation can only be performed for the nadir pixel of the two cameras at the exact time of the overflight, since all other pixels are observed under different viewing angles.

https://doi.org/10.5194/egusphere-2026-112
Preprint. Discussion started: 16 January 2026

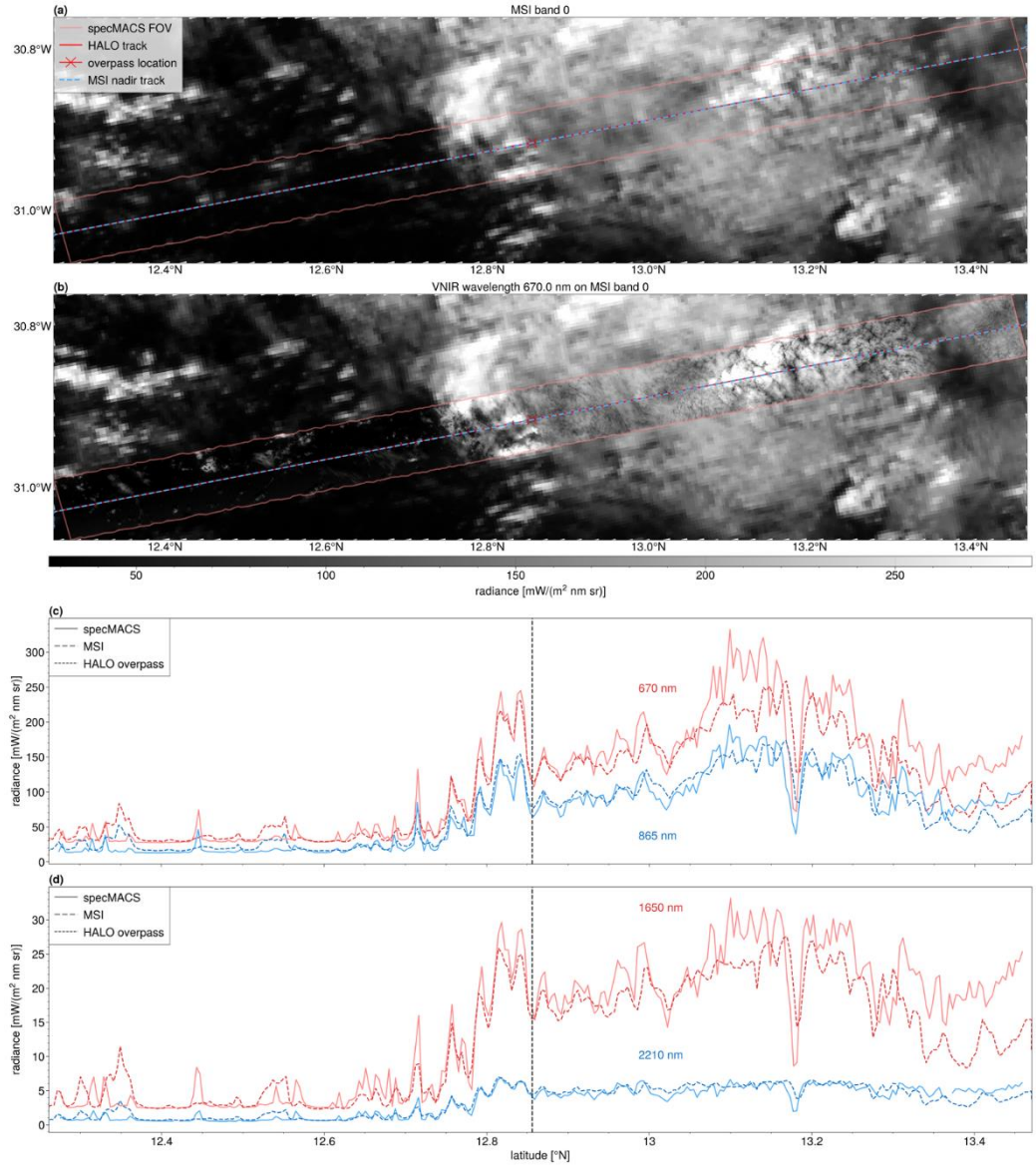

Figure 7: Comparison of specMACS to MSI on 25 August 2024. In a, the measurement of the MSI band 0 is shown for the considered measurement region. In b, the corresponding specMACS measurement at a wavelength of 670 nm is overlayed. Panels c and d show comparisons of the measured nadir pixel radiances of the two VNIR bands (panel c) and SWIR bands (panel d) with respect to the latitude. The dotted line is the overpass best match.

In the following, we consider the overflight on 25 August 2025 (01380E) with a horizontal distance of about 84 m over the tropical North Atlantic. In Figure 7, we show the 10 minutes around the overflight time for specMACS, corresponding to approximately 19 s for MSI to cover the same field of view (FOV). Figure 7a shows the radiance as seen by the visible channel of MSI. In red, the specMACS field of view is shown, while the blue dashed line depicts the nadir pixel track of the MSI band 0. The cross denotes the location of the overpass. The corresponding measurements of the 670 nm channel of the VNIR are

https://doi.org/10.5194/egusphere-2026-112
Preprint. Discussion started: 16 January 2026

overlayed on the MSI measurements in Figure 7b. Clearly, one can see the same cloud field, with a significantly higher spatial resolution of specMACS (typically around 15 m for the VNIR and less than 40 m for the SWIR at a distance of 10 km to the cloud compared to about 500 m of MSI). In Figure 7c, we show a quantitative comparison of the nadir pixels of the MSI bands 0 and 1 to the nadir pixels of the corresponding center wavelength channels of the VNIR averaged to the spatial extent of the individual MSI nadir pixels. Figure 7d shows the same for the two SWIR channels. The black dashed line depicts the time of the overpass with good agreement between specMACS and MSI around it. In general, good agreement between the two instruments is also observed for ocean pixels where time shifts between MSI and specMACS are less important. For clouds further away from the overpass time, shifts in extrema and systematic differences can be identified which are possibly due to cloud movement and development over time. Despite those smaller differences, there is a clear potential for the validation of MSI radiances with the airborne measurements of the two hyperspectral cameras of specMACS. Furthermore, L2 products, such as cloud top height, cloud phase and cloud effective radius, could be compared in the future. In particular, one could also take into account the products of the polarization resolving cameras, which use a stereographic algorithm to determine cloud geometry (Kölling et al., 2019; Volkmer et al., 2024), a new approach to derive the cloud phase (Weber et al., 2025) and measurements of the cloud bow to derive the effective radius without being subject to 3-D effects which strongly affect classical bi-spectral methods (Pörtge et al., 2023).

4.3.2 Comparison VELOX-MSI

The thermal-infrared (TIR) imager VELOX (Video airbornE Longwave Observations within siX channels; (Schäfer, et al., 2022) onboard HALO measured two-dimensional fields of brightness temperature in two broadband and four narrow-band channels with a horizontal resolution of 10 m for a HALO flight altitude of 10 km. The three VELOX channels centred at 8.7 µm, 10.7 µm and 12.0 µm were selected to match the MSI channels TIR-1 (8.8 µm), TIR-2 (10.8 µm) and TIR-3 (12.0 µm). Thus, VELOX measurements also allow nighttime validation of MSI. During the PERCUSION campaign, several flights were performed at high latitudes during twilight and night illumination conditions. On 16 November 2024, the HALO-EarthCARE underpass took place over the Norwegian Sea, where an air mass of Arctic origin was sampled. A variety of cloud structures was captured by MSI channel TIR-2 (Figure 8a). For a ±2.5-minute sequence around the underpass, a pushbroom-like image was constructed based on the 10.7 µm VELOX images and mapped on top of the MSI image (Figure 8b). In general, MSI and VELOX show similar features in the cloud structure. However, due to the dynamics of the scene a point-by-point validation is still challenging and limited to the underpass location. To allow for a fair comparison, the high spatial resolution of the VELOX measurement (12.5 m) was scaled to the MSI resolution (500 m) and spatially matched. To compensate for the dynamics of the scene, swath averages were calculated for both measurements (Figure 8c). A linear fit was applied yielding a coefficient of determination R^2 of 0.7. Reflecting the variation of clouds in the scene, the swath standard deviations are equally large for both instruments. While both platforms are moving on different time scales, the spatial distance from the underpass is a common metric for quantifying the comparability. This metric ranges between 0 km and 35 km for the ±2.5-minute VELOX sequence and is used as a color-code in Figure 8c. Directly at the underpass the swath averages show a very good

https://doi.org/10.5194/egusphere-2026-112
Preprint. Discussion started: 16 January 2026

agreement (white markers) while, with increasing distance, there are mostly distinct brightness temperature differences (darker blue and green markers) of up to 9 K. However, the cloud movement depends on the local wind pattern, which was analysed based on the auxiliary meteorological database (X-MET products, baseline AA) and the ATLID feature mask (baseline BA) to identify high and low cloud layers. In this case, higher (~ 9 km) and lower clouds (~ 2 km) experienced a southward shift caused by northerly winds and wind speeds of about 8 m s^{-1} and 17 m s^{-1}, respectively. For a 2.5-minute distance to the underpass this translates to a spatial displacement of about 1.2 km (~ 2-3 MSI pixels) for higher clouds and 2.6 km (~ 5-6 MSI pixels) for lower clouds. Nevertheless, based on the swath averages a comparison of MSI and VELOX shows a reasonable agreement. Further cases in other temperature regimes and during daytime need to be analysed to extend the potential of the MSI-VELOX validation.

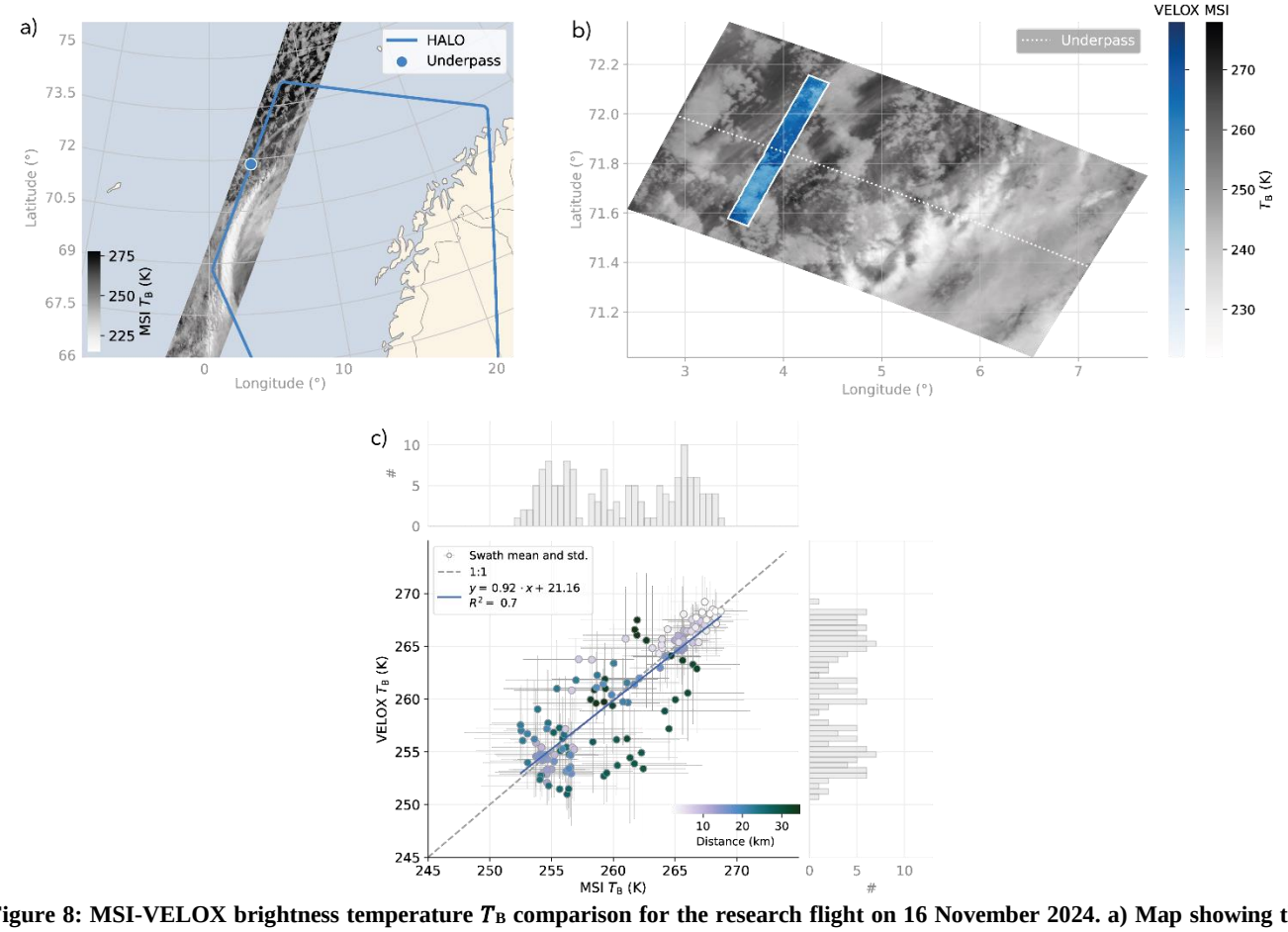

Figure 8: MSI-VELOX brightness temperature T_B comparison for the research flight on 16 November 2024. a) Map showing the HALO flight track and MSI T_B at 10.8 µm (TIR-2) for orbit 02671 frame C of baseline BA, the underpass location is marked. b) VELOX (10.7 µm) ±2.5-minute pushbroom image around the underpass mapped on top of the MSI T_B section close to the underpass. c) Comparison of MSI and VELOX swath T_B averages and standard deviations with a linear fit. Data points are colored by their spatial distance to the underpass location. Histograms of the swath T_B averages are shown at the top and right for MSI and VELOX, respectively

https://doi.org/10.5194/egusphere-2026-112
Preprint. Discussion started: 16 January 2026

4.4. BroadBand Radiometer (BBR)

For the same flight section analyzed for the VELOX-MSI comparison in Section 4.3 the BBR level 2 product BMA_FLX_2B (baseline AB) was evaluated by measurements on HALO. Due to the absence of solar radiation at these high latitudes the focus is on the thermal-infrared irradiance derived from BBR radiances. On HALO, broadband upward thermal-infrared irradiance was measured with the Broadband AirCrAft RaDiometer Instrumentation system (BACARDI; (Ehrlich et al., 2023)). The uncertainties are mostly linked to the sensitivity calibration and are in the range of 45% (2 times the standard deviation confidence level). Thermal offset effects can be neglected for this case study, because HALO did not change altitude during the flight sections. Uncertainty estimates of BBR BMA_FLX_2B irradiances (baseline BA) are released with the public release of the product by the end of 2025. However, for the section analyzed here, the BBR data status is of high to very high confidence. The comparisons of BBR and BACARDI for the 15 min flight section of the EarthCARE overpass are shown in Figure 9. The BACARDI raw data range significantly higher than BBR irradiances. This is due to the emission/absorption of thermal-IR radiation by the atmosphere above the flight altitude of HALO (here about 12.5 km). As BBR measures broadband irradiance covering significant water vapor and ozone emission/absorption lines, this needs to be considered in the comparison to BACARDI. A correction based on radiative transfer simulations using the atmospheric properties from the AUX_MET_1D product was applied to the BACARDI data. The quality of the simulations was confirmed by comparing the downward thermal-IR irradiance that has additionally been derived from the simulations and was also measured by BACARDI. The flight section averages amount to 18.96 W m^{-2} (simulations) and 19.19 W m^{-2} (BACARDI) and show negligible differences. As shown in Figure 9 (blue line), the flight altitude correction of the BACARDI measurement shifts the airborne observations close to the BBR data. The mean upward irradiance of BACARDI was corrected from 199.3 Wm^{-2} to 192.8 Wm^{-2} matching the BBR product of 186.4 Wm-2 within the uncertainty range of BACARDI. While the average irradiances agree, some deviations of the variations in the time series are obvious. This likely results from the increasing time shift between EarthCARE and HALO observations and the different footprints of the BBR and BACARDI sensors. Depending on the reference altitude of the observed scene (e.g., cloud top altitude), the hemispheric integrating optical inlet of BACARDI covers a larger area and less variability than BBR. Further studies and different cloudy and cloud-free scenes are needed to explore these effects in detail.

https://doi.org/10.5194/egusphere-2026-112
Preprint. Discussion started: 16 January 2026

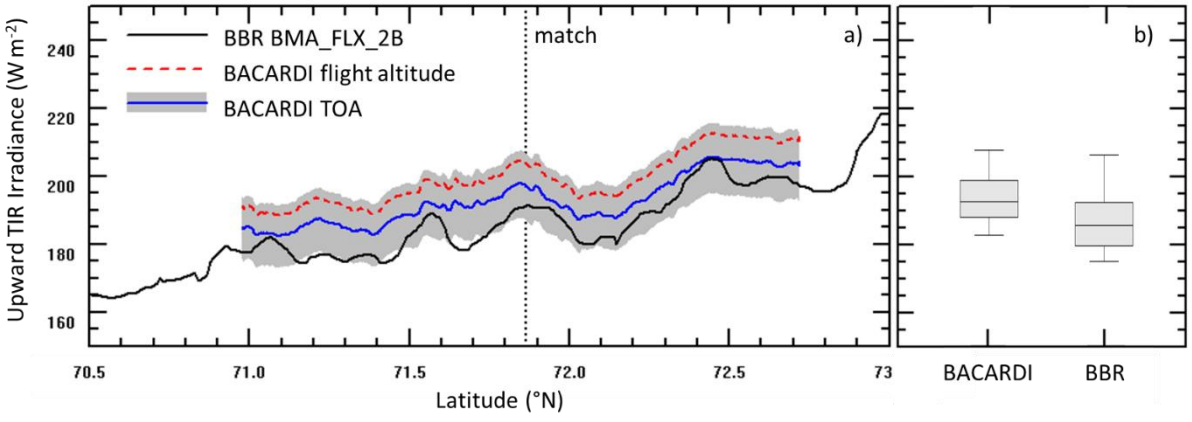

Figure 9: a) Time series (displayed as latitude) of upward thermal-IR irradiance measured by BACARDI and retrieved by BBR for 16 November 2024 (orbit 02671, frame C). Raw data and data corrected for flight altitude are displayed for BACARDI measurements. The box-wisker plot in b) show only corrected BACARDI data.

4.5. Synergy and radiative consistency

To evaluate the performance of the synergistic EarthCARE products (first data have been made publicly available Dec. 2025), we further developed independent synergistic lidar-radar retrievals (Delanoë and Hogan, 2008) to derive hight-resolved information of ice (Cazenave et al., 2019), and mixed-phase and supercooled liquid (Aubry et al., 2024) cloud microphysical properties. The retrieval is applied to lidar and radar measurements onboard HALO (Ewald et al., 2021; Aubry et al., 2024). However, although these data provide complimentary measurements and are sensitive to different moments of the particle size distribution and, thus, appear ideal for synergistic retrievals to derive particle effective size, particle number concentration, and ice/liquid water content, even using their synergy is sometimes not sufficient to constrain ice and mixed-phase cloud microphysical properties. The result of the retrieval depends strongly on the assumed particle habit and size distribution (Sourdeval et al., 2018). Measurements of the infrared (IR) emissivity (Delanoë and Hogan, 2008) or of the reflected solar radiation (Ewald et al., 2021) help to constrain the retrieved microphysical properties. Additionally, one can also use the measured radiative quantities to check the retrieved microphysical properties for consistency or to control the assumptions. The microphysical properties are retrieved using the optimal estimate framework. Next, the reflected solar radiation is simulated using the radiative transfer code (libRadtran; Mayer and Kylling, 2005) and compared with the measured solar radiation measured onboard the HALO aircraft. The same can be done using measurements onboard the EarthCARE satellite. Similarly, we can perform radiative closure for aerosol scenes, using information on microphysical properties from data bases (e.g. (Gasteiger et al., 2011; Gasteiger and Wiegner, 2018)) or from in-situ measurements (e.g. Weinzierl et al., 2011). To validate the EarthCARE products, we leverage a combination of airborne and satellite-based observations collected during PERCUSION. As an example, we performed simulations for the EarthCARE underpass on 22 August 2024, focusing on cloud free aerosol conditions. High-resolution lidar measurements of aerosol and water vapor profiles and aerosol optical properties derived from the hybrid end-to-end aerosol classification model for EarthCARE (HETEAC; Wandinger et al., 2023) were used

https://doi.org/10.5194/egusphere-2026-112
Preprint. Discussion started: 16 January 2026

as input for radiative transfer simulations. The calculated radiances were compared to measured radiances from specMACS. More precisely, broadband solar radiances were computed in the wavelength range 500–900 nm, matching the visible-near infrared (VNIR) spectral coverage of specMACS (Ewald et al., 2016). The simulations were carried out for the flight altitude and for each ~1 km nadir point along a 10 km track centred around the EarthCARE and the HALO meeting point for cloud-free (in terms of cloud) conditions. The closure revealed a good agreement with measured radiances, with a mean absolute 10 km along track difference between simulated and measured radiances of -0.07 $Wm^{-2}sr^{-1}$ (Figure 10) which corresponds to a relative difference of -0.9%. For a demonstration of how radiative consistency serves for validation and to advances the understanding of the radiative impact of the atmospheric constituents, the closure was performed with airborne observations. Once the full EarthCARE dataset will be released, this study will be extended using EarthCARE top-of-atmosphere (TOA) radiances and fluxes from the Broadband Radiometer (BBR), and including EarthCARE aerosol profiles and other atmospheric input parameters. The study will also account for new and more realistic optical properties for non-spherical dust particles.

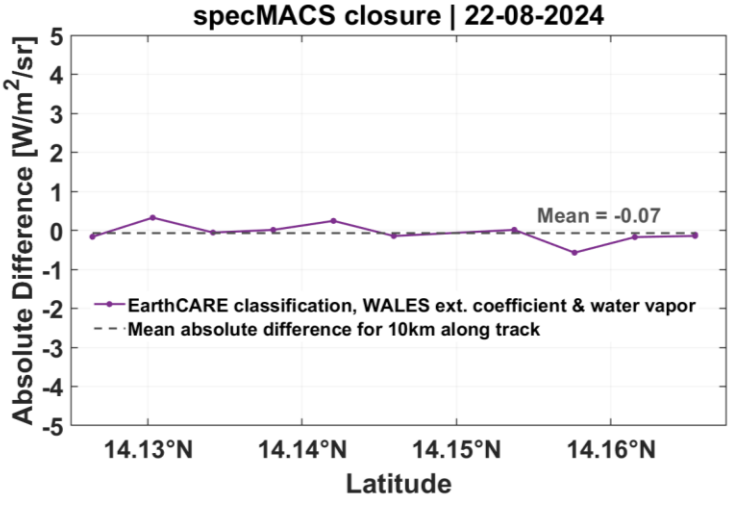

Figure 10: Differences between simulated and observed broadband SW radiances along the 10 km along track on the 22nd of August. The dashed lines denote the mean 10 km along track differences.

5. Summary and Conclusion

Airborne measurements with an EarthCARE-like payload on the German research aircraft HALO were performed during the PERCUSION campaign for scientific studies but also with the aim to validate the EarthCARE measurements and products. Validation is defined as the process of assessing the quality of data products by independent means, i.e., by data from instruments external to the mission but measuring the same geophysical quantity as the satellite sensor. We set up such an independent payload for PERCUSION and performed measurements with similar methods and viewing angles, well characterized and calibrated and with larger sensitivity and resolution (Stevens et al., 2019; Groß and Ewald, 2018). Already during preparation studies for EarthCARE (Delanoë et al., 2020) this instrumentation proved its capability and its suitability

https://doi.org/10.5194/egusphere-2026-112
Preprint. Discussion started: 16 January 2026

for validation. In addition to an independent instrumentation, we developed independent algorithms and analysis tools to validate also higher-level products.

During PERCUSION, 33 EarthCARE underpasses within 30 research flights have been performed for direct comparisons of the measurements and the derived data products from one or multi-sensor retrievals. The campaign took place during the EarthCARE commissioning phase and started with the first flight on the day EarthCARE instruments were set to operational mode. The flights were done out of three locations, Cape Verde, Barbados, and Germany in summer and fall 2024 and addressed a variety of different aerosol and cloud situations and meteorological conditions in the Sub-Tropics, Tropics, Mid- and High-Latitudes. With this intense measurement period and a sophisticated flight planning, we were able to capture all of the target scenes that have been defined as important for EarthCARE validation from a combined effort of retrieval developers and the EarthCARE Mission Advisory Group (Hall, 2025).

This study gives first intercomparison results and examples of the potential of airborne validation measurements with similar payload, highlighting different cases and data products of the EarthCARE retrieval chain. With the measurements we address a large number of the EarthCARE products either by direct validation (with similar instrumentation) or by cross-validation (e.g., using variables derived from one instrument or instrument combination to validate the derived product of another instrument). The PERCUSION measurements showed their importance especially in the very beginning of the EarthCARE mission by quickly identifying issues like cross-talk effects, background suppression or calibration uncertainties (not shown) before the data have been made publicly available. E.g. comparisons of airborne lidar measurements on HALO with ATLID can confirm the good quality of ATLID L1b data. The HALO lidar data furthermore helped to identify artefacts resulting from bugs in the layer assignment in the algorithm for the ATLID L2a optical products. With the help of the airborne data these problems could be solved quickly and the products publicly available are not affected form this issue anymore. Direct comparisons of lidar data with similar measurement technique and viewing geometry are used for the validation of the ATLID target classification. Without the uncertainties resulting from horizontal variability of the scene, the airborne measurements could identify misclassification of aerosol and cloud scenes that might have a significant impact on follow-on studies and data exploitation. Though these problems could not be completely solved, the airborne data are very valuable for algorithm improvement. Airborne radar data from PECUSION measurements helped to identify an offset of the CPR compared to MIRA measurements. A new calibration of the radar led to a much-improved data quality. The passive sensors onboard HALO furthermore confirm the general good performance of the MSI and BBR. Detailed studies are still ongoing and will be intensified with the recent release of all data products. The outcome of specific validation activities will be published in individual publications following in the next months and years.

Besides the validation of EarthCARE measurements and products and the scientific exploitation. The PERCUSION measurements are also useful for the validation of the measurements and algorithms of NASA's PACE (Plankton, Aerosol, Cloud, ocean Ecosystem) mission. We performed four dedicated flights within the swath of the PACE mission, three of them along the satellite track (Appendix A). Furthermore, with the EarthCARE-like payload on HALO, and especially with the combination of the lidar and the radar, we performed a large number of underflights under the CALIPSO and Cloudsat mission

https://doi.org/10.5194/egusphere-2026-112
Preprint. Discussion started: 16 January 2026

during past campaigns, as well as under the EarthCARE mission, and thus provide underflights under both satellite constellation and mission with combined lidar and radar payload to bridge the gap from CALIPSO/Cloudsat to EarthCARE (Appendix B).

Data availability

The EarthCARE Level-1 products and Level-2 products used in this study are publicly accessible from the ESA Earth Online gateway. The WALES measurements are available from Zenodo with DOI 10.5281/zenodo.15527242 for the Cape Verde period (Wirth 2025a), DOI 10.5281/zenodo.17153149 for the Barbados period (Wirth and Groß, 2025a), 10.5281/zenodo.17153625 for the Germany period (Wirth and Groß, 2025b). specMACS data are made available under request. HALO Radar data are available from Zenodo with DOI 10.5281/zenodo.17910007 (Ewald and Groß, 2025), and the VELOX, SMART and BACARDI data will be uploaded to the HALO-Database.

Author contribution

SG developed the outline of the paper and wrote the first draft with contributions of FE, BS, MW, GD, AE, DK, KK, SR, LV. SG developed the strategy for EarthCARE validation within PERCUSION together with BS, JW, FE, and MR. JvB, LH, RK, MPS provided the essential coordination of PERCUSION and EarthCARE. AL, BM, MW helped with the overall design of the validation campaign activities and flight planning, and are responsible for validation sub-activities within PERCUSION. All authors read the paper and discussed the findings.

Acknowledgements

We thank the flight Experiment Facility of DLR for preparing and performing the measurement flights and providing the HALO meteorological measurements. We acknowledge the contribution of Kevin Wolf, Michael Schäfer and Patrizia Schoch for operating SMART and VELOX during the flights and processing the data, of Anna Weber, Tobias Zinner, Veronika Pörtge and Anja Stallmach for the operation of specMACS and the data processing, of Sabrina Zechlau for performing flights with the WALES system, and Tanja Bodenbach for operating the WALES during flights and providing technical support, of Christian Heske, Felix Ament, and Janina Boemeke for operating the MIRA during specific flights.

Financial support

The PERCUSION campaign was partly funded by the DFG (Deutsche Forschungsgemeinschaft) within the Priority Program (Schwerpunktprogramm) SPP 1294 ‘Atmospheric and Earth System Research with HALO’ (project grant no. 316646266**)**, and by internal funding of the Max-Planck Institute for Meteorology in Hamburg, and the Institute of Atmospheric Physics of the German Aerospace Center (DLR). This study was supported by ESA under the campaign activity ‘EarthCARE: Give Airborne with Radar, Lidar –HALO EC- TOOC and Home-Base’ under ESA Contract No. 4000145500/24/NL/SC, by the Obs3RvE (Optimising 3D RT Earthcare product using geostationary observations and AI) project under Contract No.

4000147848/25/I/AG, and by the EarthCARE Data Innovation and Science Cluster (DISC) under Contract No. 4000144997/24/I-NS. The analysis of this project has further received funding from Horizon Europe programme under Grant Agreement No 101137680 via project CERTAINTY (Cloud-aERosol inTeractions & their impActs IN The earth sYstem), and by the PANGEA4CalVal project (Grant Agreement 101079201) funded by the European Union. Furthermore, the traveling to the field campaign has been supported by the DLR internal project MABAK (Innovative Methoden zur Analyse und Bewertung von Veränderungen der Atmosphäre und des Klimasystems). This research has furthermore been supported by the DFG under Grant Nos 502197012, 502188551.

Competing interests

At least one of the (co-)authors is a member of the editorial board of Atmospheric Measurement Techniques.

References

Amiridis, V., Marinou, E., Hostetler, C., Koopman, R., Cecil, D. J., Moisseev, D., . . . co-authors.: Best practices for the validation of Aerosol, Cloud, and Precipitation Profiles (ACPPV). (Zenodo, Hrsg.) doi:https://doi.org/10.5281/zenodo.15025627, 2025.

Aubry, C., Delanoe, J., Groß, S., Ewald, F., Tridon, F., Jourdan, O., and Mioche, G.: Lidar-radar synergistic method to retrieve ice, supercooled water and mixed-phase cloud properties. *Atmos. Meas. Tech., 17*, 3863--3881. doi:https://doi.org/10.5194/amt-17-3863-2024, 2024.

Barker, H. W., Korolev, A. V., Hudak, D. R., Strapp, J. W., Strawbridge, K. B., and Wolde, M.: A comparison between CloudSat and aircraft data for a multilayer, mixed phase cloud system during the Canadian CloudSat-CALIPSO Validation Project. *Journal of Geophysical Research, 113*(D00A16). doi:doi:10.1029/2008JD009971, 2008.

Bedka, K. M., Nehrir, A. R., Kavaya, M., Barton-Grimley, R., Beaubien, M., Carroll, B., . . . Skofronick-Jackson, G.: Airborne lidar observations of wind, water vapor, and aerosol profiles during the NASA Aeolus calibration and validation (Cal/Val) test flight campaign. *Atmos. Meas. Tech.s, 14*, 4305--4334. doi:https://doi.org/10.5194/amt-14-4305-2021, 2021.

Bony, S., and Stevens, B.: Measuring Area-Averaged Vertical Motions with Dropsondes. *Journal of Atmospheric Science, 76*(3), 767--783. doi:https://doi.org/10.1175/JAS-D-18-0141.1, 2019.

Burton, S. P., Ferrare, R. A., Vaughan, M. A., Omar, A. H., Rogers, R. R., Hostetler, C. A., and Hair, J. W.: Aerosol classification from airborne HSRL and comparisons with the CALIPSO vertical feature mask. *Atmos. Meas. Tech., 6*, 1397--1412. doi:https://doi.org/10.5194/amt-6-1397-2013, 2013.

Burton, S. P., Hair, J. W., Kahnert, M., Ferrare, R. A., Hostetler, C. A., Cook, A. L., . . . Rogers, R. R.: Observations of the spectral dependence of linear particle depolarization ratio of aerosols using NASA Langley airborne High Spectral Resolution Lidar. *Atmos. Chem. Phys., 15*, 13453--13473. doi:https://doi.org/10.5194/acp-15-13453-2015, 2016.

https://doi.org/10.5194/egusphere-2026-112
Preprint. Discussion started: 16 January 2026

Cazenave, Q., Ceccaldi, M., Delanoe, J., Pelon, J., Groß, S., and Heymsfield, A.: Evolution of DARDAR-CLOUD ice cloud retrievals: new parameters and impacts on the retrieved microphysical properties. *Atmos. Meas. Tech., 12*, 2819--2835. doi:https://doi.org/10.5194/amt-12-2819-2019, 2019.

Dekoutsidis, G., Wirth, M., and Groß, S.: The effects of warm air intrusions in the high arctic on cirrus clouds. *EGUsphere*., 2023.

Delanoë, J., and Hogan, R.: A variational scheme for retrieving ice cloud properties from combined radar, lidar, and infrared radiometer. *Journal of Geophysical Research, 113*(7). doi:10.1029/2007JD009000, 2008.

Delanoe, J., Ament, F., Ceccaldi, M., Groß, S., Hagen, M., Hirsch, L., . . . Vinson, J.-P.: Airborne EarthCare Preparation, Calibration and Validation Tandem System. *EarthCARE Workshop.* Tokyo. doi:https://elib.dlr.de/90952/, 2014.

Delanoë, J., Groß, S., Ewald, F., Cazenave, Q., Pelon, J., Marinou, E., and Ibrah, A.: *EPATAN project.* ESA. doi:https://doi.org/10.5270/ESA-a346352, 2020.

Donovan, D. P., Zadelhoff, G.-J. v., and Wang, P.: The EarthCARE lidar cloud and aerosol profile processor (A-PRO): the A-AER, A-EBD, A-TC, and A-ICE products. *Atmos. Meas. Tech., 17*, 5301--5340. doi:https://doi.org/10.5194/amt-17-5301-2024, 2024.

Ehrlich, A., Zöger, M., Giez, A., Nenakhov, V., Mallaun, C., Maser, R., . . . Wendisch, M.: A new airborne broadband radiometer system and an efficient method to correct dynamic thermal offsets. *Atmos. Meas. Tech., 16*, 1563--1581. doi:https://doi.org/10.5194/amt-16-1563-2023, 2023.

Eisinger, M., Marnas, F., Wallace, K., Kubota, T., Tomiyama, N., Ohno, Y., . . . Bernaerts, D.: The EarthCARE mission: science data processing chain overview. *Atmos. Meas. Tech., 17*(2), 839--862. doi:https://doi.org/10.5194/amt-17-839-2024, 2024-

Emde, C., Buras-Schnell, R., Kylling, A., Mayer, B., Gasteiger, J., Hamann, U., . . . Bugliaro, L.: The libRadtran software package for radiative transfer calculations (version 2.0.1). *Geoscientific Model Development, 9*, 1647-1672. doi:10.5194/gmd-9-1647-2016, 2016.

ESA: *Validation Needs*. Von https://earth.esa.int/eogateway/missions/earthcare/data/calibration-validation/validation-needs, 2024.

ESA: *Introducing EarthCARE's Data, Innovation and Science Cluster*. Von https://earth.esa.int/eogateway/news/introducing-earthcare-s-data-innovation-and-science-cluster, 2024.

Ewald, F., Groß, S., Hagen, M., Hirsch, L., Delanoe, J., and Bauer-Pfundstein, M.:. Calibration of a 35 GHz airborne cloud radar: lessons learned and intercomparisons with 94 GHz cloud radars. *Atmos. Meas. Tech.s, 12*, 1815-1839. doi:10.5194/amt-12-1815-2019, 2019.

Ewald, F., Groß, S., Wirth, M., Delanoe, J., Fox, S., and M. B.: Why we need radar, lidar, and solar radiance observations to constrain ice cloud microphysics. *Atmos. Meas. Tech.s, 14*(7). doi:https://doi.org/10.5194/amt-14-5029-2021, 2021.

Ewald, F., Kölling, T., Baumgartner, A., Zinner, T., and Mayer, B.: Design and characterization of specMACS, a multipurpose hyperspectral cloud and sky imager. *Atmos. Meas. Tech., 9*(5), 2015-2042. doi:10.5194/amt-9-2015-2016, 2016.

https://doi.org/10.5194/egusphere-2026-112
Preprint. Discussion started: 16 January 2026

Fix, A., Amediek, A., Ehret, G., Groß, S., Kiemle, C., Reitebuch, O., and Wirth, M.:. On the Benefit of airborne emonstrators or space borne lidar missions. (I. -I. Optics, Hrsg.) *Proc. of SPIE, Vol. 10562*. doi:doi: 10.1117/12.2296197, 2016.

Floutsi, A. A., Rizos, K., Trapon, D., Engelmann, R., Althausen, D., Marinou, E., . . . Baars, H.: On the representativeness of the ground-based lidar observations for satellite calibration/validation – the example of the archipelago of Cabo Verde. *EGUsphere*. doi:https://doi.org/10.5194/egusphere-2025-4742, 2025.

Freudenthaler, V., Esselborn, M., Wiegner, M., Heese, B., Tesche, M., Ansmann, A., . . . Seefeldner, M.:. Depolarization ratio profiling at several wavelengths in pure Saharan dust during SAMUM 2006. *Tellus B: Chemical and Physical Meteorology, 61*(1), 165--179. doi:DOI: 10.1111/j.1600-0889.2008.00396.x, 2009.

Gasteiger, J., and Wiegner, M.: MOPSMAP v1.0: a versatile tool for the modeling of aerosol optical properties. *Geoscientific Model Development, 11*(7), 2739--2018. doi:https://doi.org/10.5194/gmd-11-2739-2018, 2018.

Gasteiger, J., Wiegner, M., Groß, S., Freudenthaler, V., Toledano, C., Tesche, M., and Kandler, K.: Modelling lidar-relevant optical properties of complex mineral dust aerosols. *Tellus B: Chemical and Physical Meteorology, 63*(4), 725--741. doi:https://doi.org/10.1111/j.1600-0889.2011.00559.x, 2011, 2011.

Getzewich, B. J., Vaughan, M. A., Hunt, W. H., Avery, M. A., Powell, K. A., Tackett, J. L., . . . Toth, T. D.: CALIPSO lidar calibration at 532 nm: version 4 daytime algorithm. *Atmos. Meas. Tech., 11*, 6309--6326. doi:https://doi.org/10.5194/amt-11-6309-2018, 2018.

Giez, A. Z., Mallaun, C., Nenakhov, V., Schimpf, M., Grad, C., Numberger, A., and Raynor, K.: Determination of the Measurement Errors for the HALO Basic Data System BAHAMAS by Means of Error Propagation. (D. Z.-u. Raumfahrt, Hrsg.) *DLR-Forschungsbericht*. doi:10.57676/5rdc-q708, 2023.

Groß, S., and Ewald, F.: *NARPEX project - Final Report.* DLR. Von https://elib.dlr.de/216858/, 2018.

Groß, S., Esselborn, M., Weinzierl, B., Wirth, M., Fix, A., and Petzold, A.: Aerosol classification by airborne high spectral resolution lidar observations. *Atmospheric Chemistriy and Physics, 13*, 2487–2505. doi:10.5194/acp-13-2487-2013, 2013.

Groß, S., Freudenthaler, V., Haarig, M., Ansmann, A., Toledano, C., Mateos, D., . . . Weinzierl, B.: Characterization of aerosol over the eastern Mediterranean by polarization-sensitive Raman lidar measurements during A-LIFE – aerosol type classification and type separation. *Atmos. Chem. Phys., 25*, 3191--3211. doi:https://doi.org/10.5194/acp-25-3191-2025, 2025.

Groß, S., Freudenthaler, V., Schepanski, K., Toledano, C., Schäfler, A., Ansmann, A., and Weinzierl, B.: Optical properties of long-range transported Saharan dust over Barbados as measured by dual-wavelength depolarization Raman lidar measurements. *Atmos. Chem. Phys., 15*, 11067--11080. doi:https://doi.org/10.5194/acp-15-11067-2015, 2015.

Groß, S., Freudenthaler, V., Wirth, M., and Weinzierl, B.: Towards an aerosol classification scheme for future EarthCARE lidar observations and implications for research needs. *Atmospheric Science Letter, 16*, 77--82. doi:https://doi.org/10.1002/asl2.524, 2015.

https://doi.org/10.5194/egusphere-2026-112
Preprint. Discussion started: 16 January 2026

Groß, S., Tesche, M., Freudenthaler, V., Toledano, C., Wiegner, M., Ansmann, A., . . . Seefeldner, M.:. Characterization of Saharan dust, marine aerosols and mixtures of biomass-burning aerosols and dust by means of multi-wavelength depolarization and Raman lidar measurements during SAMUM 2. *Tellus B: Chemical and Physical Meteorology, 63*(4), 706--724. doi:https://doi.org/10.1111/j.1600-0889.2011.00556.x, 2011.

Groß, S., Wirth, M., Schäfler, A., Fix, A., Kaufmann, S., and Voigt.: Potential of airborne lidar measurements for cirrus cloud studies. *Atmos. Meas. Tech., 7*, 2745–2755., 2014.

Gutleben, M., Groß, S., and Wirth, M.: Cloud macro-physical properties in Saharan-dust-laden and dust-free North Atlantic trade wind regimes: a lidar case study. *Atmos. Chem. Phys., 19*, 10659-10673. doi:10.5194/acp-19-10659-2019, 2019

Gutleben, M., Groß, S., Heske, C., and Wirth, M.: Wintertime Saharan dust transport towards the Caribbean: an airborne lidar case study during EUREC4A. *Atmos. Chem. Phys., 22*, 7319--7330. doi:https://doi.org/10.5194/acp-22-7319-2022, 2022

utleben, M., Groß, S., Wirth, M., and Mayer, B.: Radiative effects of long-range-transported Saharan air layers as determined from airborne lidar measurements, Atmos. Chem. Phys., 20, 12313–12327, https://doi.org/10.5194/acp-20-12313-2020, 2020.

Gutleben, M., Groß, S., Wirth, M., Emde, C., and Mayer, B.: Impacts of water vapor on Saharan air layer radiative heating. *Geophysical Research Letters, 46*, 14854--14862. doi:https://doi.org/10.1029/2019GL085344, 2019.

Haarig, M., Ansmann, A., Engelmann, R., Baars, H., Toledano, C., Torres, B., . . . Wandinger, U.: First triple-wavelength lidar observations of depolarization and extinction-to-backscatter ratios of Saharan dust. *Atmos. Chem. Phys., 22*, 355--369. doi:https://doi.org/10.5194/acp-22-355-2022, 2022.

Hair, J. W., Hostetler, C. A., Ferrare, R. A., Cook, A. L., and Harper, D. B.:. The NASA Langley airborne high spectral resolution lidar for measurements of aerosols and clouds. *Reviewed and Revised Papers Presented at the 23rd International Laser Radar Conference* (S. 411--414). Tokyo: Tokyo Metropolitan University. https://laser-sensing.jp/ilrc23_CD1a2b3c/ILRC23/3P-5.pdf, 2006.

Hall, A.: *EarthCARE Validation – Level 2 Algorithm Developer Needs*, https://earth.esa.int/eogateway/documents/d/earth-online/earthcare-validation-l2-algorithm-developer-needs-table, 2005

IPCC: *Climate Change 2021 – The Physical Science Basis.* (I. P. (IPCC), Hrsg.) Cambridge University Press. doi:https://doi.org/10.1017/9781009157896, 2023.

Kacenelenbogen, M., Redemann, J., Vaughan, M. A., Omar, A. H., Russell, P. B., Burton, S., . . . Hostetler, C. A.: An evaluation of CALIOP/CALIPSO's aerosol-above-cloud detection and retrieval capability over North America. *Journal of Geophysical Research: Atmosphere, 119*, 230--244. doi:doi:10.1002/2013JD020178, 2014.

Kar, J., Vaughan, M. A., Lee, K.-P., Tackett, J. L., Avery, M. A., Garnier, A., . . . Winker, D. M.:. CALIPSO lidar calibration at 532 nm: version 4 nighttime algorithm. *Atmos. Meas. Tech., 11*, 1459--1479. doi:https://doi.org/10.5194/amt-11-1459-2018, 2018.

https://doi.org/10.5194/egusphere-2026-112
Preprint. Discussion started: 16 January 2026

King, M. D., Menzel, W. P., Granz, P. S., Myers, J. S., Arnold, G. T., Gumley, L. E., . . . Osterwisch, F. G.: Airborne Scanning Spectrometer for Remote Sensing of Cloud, Aerosol, Water Vapor, and Surface Properties. *Journal of Atmospheric and Oceanic Technology, 13*(4), 777--794. doi:https://doi.org/10.1175/1520-0426(1996)013<0777:ASSFRS>2.0.CO;2, 1996.

Kölling, T., Zinner, T., and Mayer, B.:. Aircraft-based stereographic reconstruction of 3-D cloud geometry. *Atmospheric Measurements Techniques, 12*, 1155--1166. doi:https://doi.org/10.5194/amt-12-1155-2019, 2019.

Koopmann, R.:. *Scientific Validation Implementation Plan*, https://earth.esa.int/eogateway/documents/d/earth-online/earthcare-scientific-validation-implementation-plan, 2024

Krautstrunk, M., and Giez, A.: The Transition From FALCON to HALO Era Airborne Atmospheric Research. *Atmospheric Physics: Background-Methods-Trends*, 609--624, doi:https://doi.org/10.1007/978-3-642-30183-4_37https://doi.org/10.1007/978-3-642-30183-4_37, 2012.

Lemmerz, C., Lux, O., Witschas, B., Rahm, S., Marksteiner, U., Geiß, A., . . . Reitebuch, O.:. Airborne Doppler wind LIDAR technology demonstration for Aeolus: from pre-launch campaigns to mission performance validation. *Proc. SPIE 12777, International Conference on Space Optics — ICSO 2022, 1277707*. doi:https://doi.org/10.1117/12.2688591, 2023.

Lux, O., Lemmerz, C., Weiler, F., Marksteiner, U., Witschas, B., Rahm, S., . . . Reitebuch, O.: Airborne wind lidar observations over the North Atlantic in 2016 for the pre-launch validation of the satellite mission Aeolus. *Atmos. Meas. Tech., 11*, 3297--3322. doi:https://doi.org/10.5194/amt-11-3297-2018, 2018.

Lux, O., Lemmerz, C., Weiler, F., Marksteiner, U., Witschas, B., Rahm, S., . . . Reitebuch, O.: Retrieval improvements for the ALADIN Airborne Demonstrator in support of the Aeolus wind product validation. *Atmos. Meas. Tech., 15*, 1303--1331. doi:https://doi.org/10.5194/amt-15-1303-2022, 2022.

Marinou, E., Amiridis, V., Paschou, P., Tsekeri, A., Tsikoudi, I., and Voudouri, K.-A.: Across Mediterranean Experiment for the Cal/Val of the Earthcare Mission. *IGARSS 2024 - 2024 IEEE International Geoscience and Remote Sensing Symposium*. doi:10.1109/IGARSS53475.2024.10642456, 2024.

Marinou, E., Ewald, F., Gross, S., Wirth, M. S., Cazenave, Q., and Delanoe, J.: Aerosol-Cloud Target Classification in HALO Lidar/Radar Collocated Measurements. *EPJ Web of Conferences, 237*, 08002. doi:https://doi.org/10.1051/epjconf/202023708002, 2020.

Mayer, B., and Kylling, A.: Technical note: The libRadtran software package for radiative transfer calculations - description and examples of use. *Atmos. Chem. Phys., 5*, 1855--1877. doi:https://doi.org/10.5194/acp-5-1855-2005, 2005.

McGill, M. J., Vaughan, M. A., Trepte, C. R., Hart, W. D., Hlavka, D. L., Winker, D. M., and Kuehn, R.: Airborne validation of spatial properties measured by the CALIPSO lidar. *Journal of Geophysical Research, 112*(D20201). doi:doi:10.1029/2007JD008768, 2007.

https://doi.org/10.5194/egusphere-2026-112
Preprint. Discussion started: 16 January 2026

Mech, M., Orlandi, E., Crewell, S., Ament, F., L., H., Hagen, M., . . . Stevens, B.: HAMP – the microwave package on the High Altitude and LOng range research aircraft (HALO). *Atmos. Meas. Tech.*, *7*(12), 4539-4553. doi:10.5194/amt-7-4539-2014, 2014.

Paffrath, U., Lemmerz, C., Reitebuch, O., Witschas, B., Nikolaus, I., and Freudenthaler, V.: The Airborne Demonstrator for the Direct-Detection Doppler Wind Lidar ALADIN on ADM-Aeolus. Part II: Simulations and Rayleigh Receiver Radiometric Performance. *Journal of Atmospheric and Ocean Technology, 26*, 2516--2530. doi:https://doi.org/10.1175/2009JTECHA1314.1, 2009.

Pörtge, V., Kölling, T., Weber, A., Volkmer, L., Emde, C., Zinner, T., . . . Mayer, B.:. High-spatial-resolution retrieval of cloud droplet size distribution from polarized observations of the cloudbow. *Atmos. Meas. Tech., 6*, 645--667. doi:https://doi.org/10.5194/amt-16-645-2023, 2023.

Puigdomènech Treserras, B., Kollias, P., Battaglia, A., Tanelli, S., and Nakatsuka, H.: EarthCARE's cloud profiling radar antenna pointing correction using surface Doppler measurements, Atmos. Meas. Tech., 18, 5607–5618, https://doi.org/10.5194/amt-18-5607-2025, 2025.

Reitebuch, O., Lemmerz, C., Nagel, E., Paffrath, U., Durand, Y., Endemann, M., . . . Chaloupy, M.: The Airborne Demonstrator for the Direct-Detection Doppler Wind Lidar ALADIN on ADM-Aeolus. Part I: Instrument Design and Comparison to Satellite Instrument. *Journal of Atmospheric and Ocean Technology, 26*, 2501--2515. doi:https://doi.org/10.1175/2009JTECHA1309.1, 2009.

Rogers, R. R., Ferrare, R. A., Liu, Z., Obland, M. D., Harper, D. B., Cook, A. L., . . . Winker, D. M.: Assessment of the CALIPSO Lidar 532 nm attenuated backscatter calibration using the NASA LaRC airborne High Spectral Resolution Lidar. *11*, 1295--1311. doi:https://doi.org/10.5194/acp-11-1295-2011, 2011.

Rogers, R. R., Vaughan, M. A., Hostetler, C. A., Burton, S. P., Ferrare, R. A., Young, S. A., . . . Winker, D. M.:. Looking through the haze: evaluating the CALIPSO level 2 aerosol optical depth using airborne high spectral resolution lidar data. *Atmos. Meas. Tech., 7*, 4317--4340. doi:https://doi.org/10.5194/amt-7-4317-2014, 2014.

Röttenbacher, J., Ehrlich, A., Müller, H., Ewald, F., Luebke, A. E., Kirbus, B., . . . Wendisch, M.: Evaluating the representation of Arctic cirrus solar radiative effects in the Integrated Forecasting System with airborne measurements. *Atmos. Chem. Phys., 24*, 8085--8104. doi:https://doi.org/10.5194/acp-24-8085-2024, 2024.

Schäfer, M., Wolf, K., Ehrlich, A., Hallbauer, C., Jäkel, E., Jansen, F., . . . Wendisch, M.: VELOX – a new thermal infrared imager for airborne remote sensing of cloud and surface properties. *Atmos. Meas. Tech., 15*(5), 1491-1509. doi:10.5194/amt-15-1491-2022, 2022.

Schäfler, A., and Coauthors:. The North Atlantic Waveguide and Downstream Impact Experiment. *Bulletin of the American Meteorological Society, 99*, 1607--1637. doi:https://doi.org/10.1175/BAMS-D-17-0003.1, 2018.

Sourdeval, O., Gryspeerdt, E., Krämer, M., Goren, T., Delanoë, J., Afchine, A., . . . Quaas, J.: Ice crystal number concentration estimates from lidar–radar satellite remote sensing – Part 1: Method and evaluation. *Atmos. Chem. Phys., 18*, 14327--14350. doi: https://doi.org/10.5194/acp-18-14327-2018, 2018.

https://doi.org/10.5194/egusphere-2026-112
Preprint. Discussion started: 16 January 2026

Stephens, G. L., Vane, D. G., S, T., Im, E., Durden, S., Rokey, M., . . . Marchand, R.: CloudSat mission: Performance and early science after the first year of operation. *Journal of Georphysical Research: Atmosphere, 113*(D8). doi: https://doi.org/10.1029/2008JD009982, 2008.

Stephens, G., Winker, D., Pelon, J., Trepte, C., Vane, D., Yuhas, C., . . . Lebsock, M.:. CloudSat and CALIPSO within the A-Train: Ten Years of Actively Observing the Earth System. *Bulletin of the American Meteorological Society*, 569--581. doi:https://doi.org/10.1175/BAMS-D-16-0324.1., 2018.

Stevens, B., Ament, F., Bony, S., Crewell, S., Ewald, F., Gross, S., . . . Farrell, D.: A High-Altitude Long-Range Aircraft Configured as a Cloud Observatory: The NARVAL Expeditions. *Bullentin of the American Meteorological Society, 100*(6), 1061-1077, https://journals.ametsoc.org/view/journals/bams/100/6/bams-d-18-0198.1.xml, 2019.

Stevens, B., Bony, S., Gross, S., Klocke, D., Windmiller, J., Wing, A. A., . . . Wu, Y.: ORCESTRA: Organized Convection and EarthCARE Studies over the Tropical Atlantic. *Tellus B, in review, 2026*

Stevens, B., Farrell, D., Hirsch, L., Jansen, F., Nuijens, L., Serikov, I., . . . Prospero, J. M.: The Barbados Cloud Observatory: Anchoring Investigations of Clouds and Circulation on the Edge of the ITCZ. *Bulletin of the American meteorological Society, 97*(5), 787--801. doi:https://doi.org/10.1175/BAMS-D-14-00247.1, 2016.

Urbanek, B., Groß, S., Schäfler, A., and Wirth, M.: Determining stages of cirrus evolution: a cloud classification scheme. *Atmos. Meas. Tech., 10*, 1653–1664, 2017.

Volkmer, L., Kölling, T., Zinner, T., and Mayer, B.: Consideration of the cloud motion for aircraft-based stereographically derived cloud geometry and cloud top heights. *Atmos. Meas. Tech., 17*, 6807--6817. doi:https://doi.org/10.5194/amt-17-6807-2024, 2024.

Wandinger, U., Floutsi, A. A., Baars, H., Haarig, M., Ansmann, A., Hünerbein, A., . . . Cole, J.: HETEAC – the Hybrid End-To-End Aerosol Classification model for EarthCARE. *Atmos. Meas. Tech., 16*, 2485--2510. doi:https://doi.org/10.5194/amt-16-2485-2023, 2023.

Wandinger, U., Haarig, M., Baars, H., Donovan, D., and van Zadelhoff, G.-J.: Cloud top heights and aerosol layer properties from EarthCARE lidar observations: the A-CTH and A-ALD products. *Atmos. Meas. Tech., 16*, 4031--4052. doi:https://doi.org/10.5194/amt-16-4031-2023, 2023.

Weber, A., Kölling, T., Pörtge, V., Baumgartner, A., Rammeloo, C., Zinner, T., and Mayer, B.:. Polarization upgrade of specMACS: calibration and characterization of the 2D RGB polarization-resolving cameras. *Atmos. Meas. Tech., 17*, 1419--1439. doi:https://doi.org/10.5194/amt-17-1419-2024, 2024.

Weber, A., Pörtge, V., Emde, C., and Mayer, B.: Retrieval of cloud thermodynamic phase partitioning from multi-angle polarimetric imaging of Arctic mixed-phase clouds, Atmos. Meas. Tech., 18, 7581–7601, https://doi.org/10.5194/amt-18-7581-2025, 2025.

Wehr, T., Kubota, T., Tzeremes, G., Wallace, K., Nakatsuka, H., Ohno, Y., . . . Bernaerts, D.: The EarthCARE mission – science and system overview. *Atmos. Meas. Tech.s, 16*(15), 3581--3608. doi:https://doi.org/10.5194/amt-16-3581-2023, 2023.

https://doi.org/10.5194/egusphere-2026-112
Preprint. Discussion started: 16 January 2026

Weinzierl, B., Sauer, D., Esselborn, M., Petzold, A., Veira, A., Rose, M., . . . Freuntenthaler, V.: Microphysical and optical properties of dust and tropical biomass burning aerosol layers in the Cape Verde region—an overview of the airborne in situ and lidar measurements during SAMUM-2. *Tellus B: Chemical and Physical meteorology, 4*, 589--618. doi:https://doi.org/10.1111/j.1600-0889.2011.00566.x, 2011.

Winker, D. M., Pelon, J., Coakley, J. A., Ackerman, S. A., Charlson, R. J., Colarco, P. R., . . . Wielicki: The Calipso Mission: A Global 3D View of Aerosols and Clouds. *Bulletin of the American Meteorological Society, 91*(9), 1211--1230. doi:https://doi.org/10.1175/2010BAMS3009.1, 2010.

Wirth, M., Fix, A., Mahnke, P., Schwarzer, H., Schrandt, F., and Ehret, G.: The airborne multi-wavelength water vapor differential absorption lidar WALES: system design and performance. *Applied Physics B, 96*, 201-213. doi:10.1007/s00340-009-3365-7, 2009.

Witschas, B., Lemmerz, C., Geiß, A., Lux, O., Marksteiner, U., Rahm, S., . . . Weiler, F.: First validation of Aeolus wind observations by airborne Doppler wind lidar measurements. *Atmos. Meas. Tech., 13*, 2381--2369. doi:https://doi.org/10.5194/amt-13-2381-2020, 2020.

Witschas, B., Lemmerz, C., Geiß, A., Lux, O., Marksteiner, U., Rahm, S., . . . Weiler, F.: Validation of the Aeolus L2B wind product with airborne wind lidar measurements in the polar North Atlantic region and in the tropics. *Atmos. Meas. Tech., 15*, 7049--7070. doi:https://doi.org/10.5194/amt-15-7049-2022, 2022.

Wolf, K., Ehrlich, A., Mech, M., Hogan, R. J., and Wendisch, M.: Evaluation of ECMWF Radiation Scheme Using Aircraft Observations of Spectral Irradiance above Clouds. *Journal of Atmospheric Science, 77*, 2665--2685. doi:https://doi.org/10.1175/jas-d-19-0333.1, 2020.

https://doi.org/10.5194/egusphere-2026-112
Preprint. Discussion started: 16 January 2026

Appendix A: PACE-Validation

The focus of the PERCUSION campaign was clearly on the validation of EarthCARE. However, our flight schedule and measurement strategy allowed also to underfly NASA's PACE (Plankton, Aerosol, Cloud, ocean Ecosystem) mission during four measurement flights out of Barbados. PACE (NASA PACE - Home) was launched on 8 February 2024 and aims to extend the data record of ocean colour, aerosol and cloud data for Earth systems studies as well as to address new and emerging science questions. For that, PACE is equipped with the Ocean Color Instrument (OCI) and the Multi-angle Polarimeters HARP2 and SPEXone. The maximum swath width is about 2500 km for the OCI, 1500 km for HARP2, and 100 km for SPEXone. Any measurements within the swath width of the satellite is thus valuable for validation. Figure A1 gives an overview of the flight scene from a lidar perspective for the different days a underpass was performed or HALO was measuring within the swath of PACE. Over measurements covered a variaty of different conditions from background marine aerosol conditions, over midlevel stratiform clouds, thin cirrus condition, cirrus clouds, to clouds of deep convective systems. With that our measurements not only seve for direct comparisons of the polarimeter measurements using the specMACS data, but also for the verification of the atmospheric model to investigate the impact of aerosol and clouds on PACE measurements. For the latter especially the vertical information from lidar and radar as well as their synergistic use to derive microphysical cloud properties is of interest. Table A1 gives information on date and time of the underpasses.

Table A1: Information of date, time and location of HALO measurements along or in the PACE tack.

Date	Best Match Time (UTC)	Time on track (UTC)	Best Match Distance (km)
7 September 2024	16 :00	17:10 – 17:39	89.9
16 September 2024	16 :15	16:02 – 16:43	1.0
19 September 2024	16 :22	15:45 – 16:27	0.6
28 September 2024	16 :35	16:23 – 17:30	21.5

https://doi.org/10.5194/egusphere-2026-112
Preprint. Discussion started: 16 January 2026

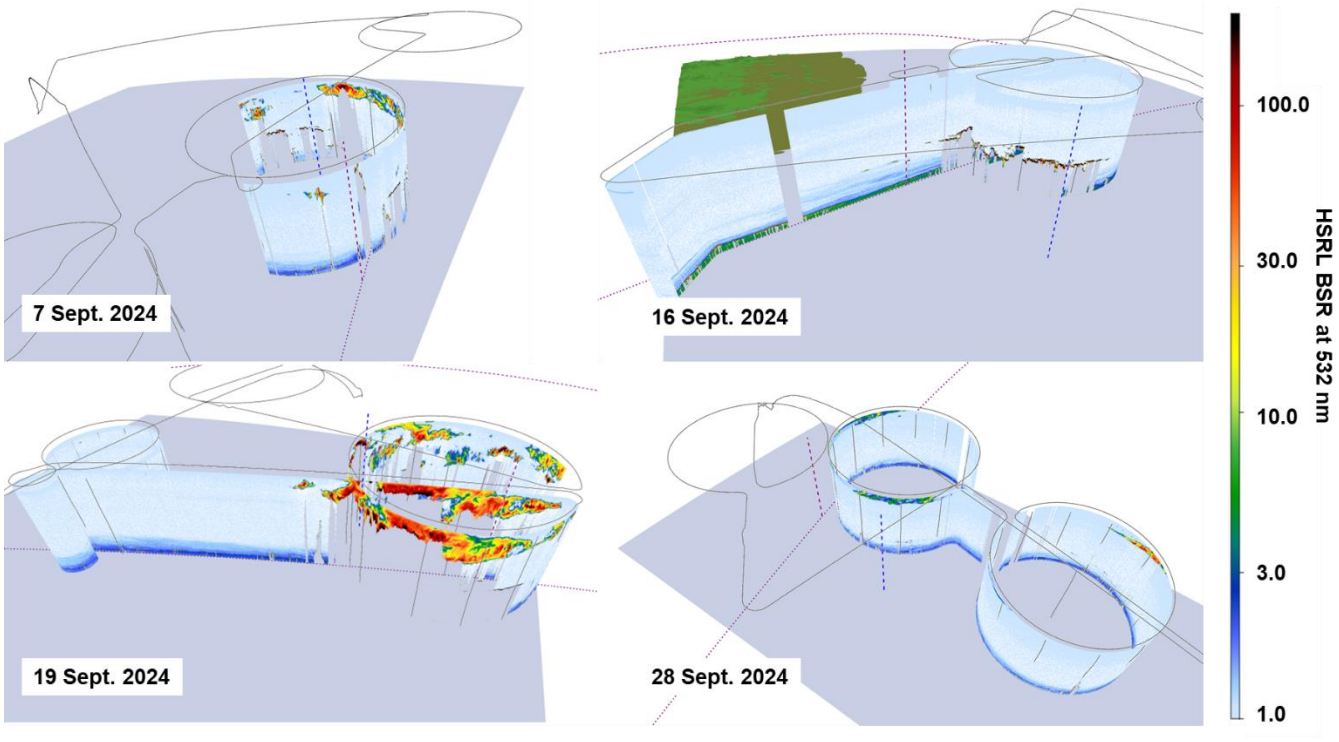

Figure A1: Cross-section of the backscatter ratio at 532 nm from WALES measurements for the four underpasses within the PACE track. The dashed red lines indicate the nearest PACE measurement in time, the blue dashed line indicate the nearest EarthCARE measurement in time.

https://doi.org/10.5194/egusphere-2026-112
Preprint. Discussion started: 16 January 2026

Appendix B: Bridging the gap from CALIPSO/Cloudsat to EarthCARE

CALIPSO and Cloudsat provided a large opportunity to study aerosol, clouds, their interaction and their impact on radiation and precipitation. This will be continued with EarthCARE. However, going from CALIPSO/Cloudsat to Earth CARE, we do not only have a change in lidar wavelength and technique, but also a change in sensitivity and resolution for both, lidar and radar. Unfortunately, both satellite constellations did not have a direct overlap, making it difficult to directly link the two time-series and data sets. Collocated measurements with both, the CALIPSO/Cloudsat constellation and with EarthCARE, are needed to bridge that gap. Next to continuing ground-based lidar and radar measurements which provide long-term measurements but with limited overlap, collocated airborne measurements with lidar and radar provide a valuable contribution. The largest number of CALIPSO underflights is certainly provided by the NASA Langley lidar group with their HSRL/HSRL-2 system (Hair et al., 2006). After the launch of EarthCARE, they also performed EarthCARE underpasses for the validation of the ATLID. However, with our combined active (lidar and radar) and passive remote sensing payload (Stevens, et al., 2019) we address to bridging both; the lidar and radar measurements from CALIPSO/Cloudsat and EarthCARE underpasses. Table B.1 gives an overview of our performed CALIPSO/Cloudsat unterflights.

https://doi.org/10.5194/egusphere-2026-112
Preprint. Discussion started: 16 January 2026

Table B1: Information on date, region, time flight mission and measurement conditions for CALIPSO/Cloudsat underpasses with the same lidar and radar instruments used during PERCUSION.

Date	Flight region	Time of collocation [UTC]	Flight mission	Condition
24 Jul. 2013	Germany	12:18	NARVAL (test)	Thin cirrus clouds Continental background aerosol
10 Dec. 2013	North Atlantic	15:08	NARVAL (south)	Low level precipitating clouds Marine aerosol
11 Dec. 2013	Sub-tropical North Atlantic	17:26	NARVAL (south)	Marine aerosol Shallow marine convection
12 Dec 2013	Sub-tropical North Atlantic	16:30	NARVAL (south)	Marine aerosol Shallow and stratiform clouds
14 Dec. 2013	Sub-tropical North Atlantic	16:18	NARVAL (south)	Marine aerosol Shallow convection, partly precipitating
15 Dec. 2013	Sub-tropical North Atlantic	17:01	NARVAL (south)	Marine aerosol Shallow convection, partly precipitating
16 Dec. 2013	Sub-tropical North Atlantic	16:07	NARVAL (south)	Marine aerosol Shallow convection, partly precipitating
20 Dec. 2013	North Atlantic	17:23	NARVAL (south)	Marine aerosol Shallow convection
9 Jan. 2014	Extra-tropical North Atlantic	15:29	NARVAL (north)	Marine aerosol Scattered low level clouds, partly precipitating
18 Jan. 2014	Extra-tropical North Atlantic	13:44	NARVAL (north)	Deep convective clouds, ice anvils, frontal bands
21 Jan. 2014	Extra-tropical North Atlantic	14:19	NARVAL (north)	High and convective clouds Marine aerosol
10 Aug. 2016	Sub-tropical North Atlantic	17:09	NARVAL-II	Low to mid-level clouds, partly precipitating Marine aerosol and Saharan dust
15 Aug. 2016	Sub-tropical North Atlantic	17:10	NARVAL-II	Stratiform and upper-level clouds Marine aerosol and Saharan dust
17 Aug. 2016	Sub-tropical North Atlantic	17:01	NARVAL-II	Low level and cirrus clouds Marine aerosol and dust mixture
19 Aug. 2016	Sub-tropical North Atlantic	16:47	NARVAL-II	Shallow marine convection Marine aerosol, Saharan dust and dust mixture
14 Oct. 2016	Extra-tropical North Atlantic	12:53	NAWDEX	Deep convection, precipitation, stratiform clouds Marine aerosol